2	trunk stabilization
3	
4	
5	
6	
7 8	Bharadwaj Nandakumar a,b¹, Gary H. Blumenthal a,b¹, Francois Philippe Pauzin b, Karen A Moxon a,b,c
9	<sup>1</sup> these two authors contributed equally
LO L1	a. Department of Biomedical Engineering, Science, and Health Systems, Drexel University, Philadelphia, PA.
L2	b. Department of Biomedical Engineering, University of California Davis, Davis, CA
L3	c. Center for Neuroscience, Davis, CA
L4	
L5	
L6	
L7	
L8	
L9	Corresponding Author:
20	Karen A. Moxon, PhD
21	+1-530-752-8156
22	Moxon@ucdavis.edu
23	University of California, Davis
24	451 E. Health Sciences Drive
25	GBSF 3321
26	Davis, CA 95616
27	
28	

29 Abstract

Sensorimotor integration in the trunk system is poorly understood despite its importance for
functional recovery after neurological injury. To address this, a series of mapping studies were
performed in the rat. First, the receptive field (RF) of cells recorded from thoracic dorsal root
ganglia were identified. Second, the RF of cells recorded from trunk primary sensory cortex (S1)
were used to assess the extent and internal organization of trunk S1. Finally, the trunk motor
cortex (M1) was mapped using intracortical microstimulation to assess coactivation of trunk
muscles with hindlimb and forelimb muscles, and integration with S1. Projections from trunk S1
to trunk M1 were not anatomically organized, with relatively weak sensorimotor integration
between trunk S1 and M1 compared to extensive integration between hindlimb S1/M1 and trunk
M1. Assessment of response latency and anatomical tracing suggest that trunk M1 is abundantly
guided by hindlimb somatosensory information that is derived primarily from the thalamus.
Finally, neural recordings from awake animals during unexpected postural perturbations support
sensorimotor integration between hindlimb S1 and trunk M1, providing insight into the role of
the trunk system in postural control that is useful when studying recovery after injury.

44 Keywords: dermatome, dorsal root ganglion, motor cortex, mapping, sensory cortex

46 Significance

This work identifies extensive sensorimotor integration between trunk and hindlimb cortices, demonstrating that sensorimotor integration is an operational mode of the trunk cortex in intact animals. The function of this integration was demonstrated for postural control when the animal was subjected to lateral tilts. Furthermore, these results provide insight into cortical

reorganization after spinal cord injury (SCI) and suggest that sensorimotor integration after SCI is an attempt to restore sensorimotor integration that existed in the intact system. These results could be used to tailor rehabilitative strategies to optimize sensorimotor integration for recovery of function.

56 Classification

57 Biological sciences, neuroscience

# 59 Introduction

60	Transmission of information between somatosensory and motor systems, or sensorimotor
61	integration, is crucial for perception (Mao et al. 2011) and volitional control of movement
62	(Rossignol et al. 2006). Understanding the substrates of sensorimotor integration is important for
63	studies examining locomotor function. For example, sensorimotor integration has been
64	extensively studied in the rodent whisker system (Farkas et al. 1999; Ferezou et al. 2007;
65	Chakrabarti et al. 2008; Megevand et al. 2009; Mao et al. 2011; Hooks et al. 2013; Smith and
66	Alloway 2013) giving rise to a better understanding of how rodents use their whiskers optimally
67	to navigate and discriminate features of their environment. Furthermore, research on the forelimb
68	(Asanuma et al. 1968; Chapin 1986; Tutunculer et al. 2006; Morales-Botello et al. 2012; Kunori
69	and Takashima 2016) and hindlimb systems (Hall and Lindholm 1974; Donoghue et al. 1979;
70	Hummelsheim and Wiesendanger 1985; Ghosh et al. 2009; Kao et al. 2009) has highlighted the
71	importance of sensorimotor integration for appropriate locomotor function. These studies found
72	extensive integration between anatomically and topographically corresponding sensory and
73	motor cortices, with little cross-region integration (e.g., integration between whisker sensory and
74	hindlimb motor cortices). Yet, little is known about sensorimotor integration within the trunk
75	cortex or between the trunk motor cortex and other sensory cortices, which can be of
76	fundamental importance for studies examining learning and recovery after neurological injury or
77	disease.
78	Classic mapping studies of the rodent primary sensory cortex (S1) and primary motor cortex
79	(M1) have roughly outlined the location and border of trunk S1 and M1 (Welker 1971; Hall and
80	Lindholm 1974; Chapin and Lin 1984). More recently, subregions of trunk S1 have been
81	identified, including a ventral trunk representation (Xerri et al. 1994; Seelke et al. 2012) and a

genital representation (Lenschow and Brecht 2018). Despite these findings, the internal somatotopy of trunk S1 remains ill defined, in part, due to the limited assessment of spinal dermatomes of the thoracic regions (Lombard et al. 1979; Takahashi et al. 1994). Similarly, trunk M1 is mentioned in most mapping studies (Donoghue and Wise 1982; Gioanni and Lamarche 1985; Neafsey et al. 1986) and some information has emerged from recent studies examining cortical reorganization after spinal cord injury (Giszter et al. 1998, 2008; Tandon et al. 2013; Oza and Giszter 2014, 2015; Ganzer et al. 2016; Manohar et al. 2017). However, little is known about the internal somatotopy of trunk M1 (Giszter et al. 2008; Tandon et al. 2013; Oza and Giszter 2015; Ganzer et al. 2016). Further study of the somatotopy of trunk S1 and M1, as well as how these cortices integrate information, is needed to understand the role of trunk cortex more fully, both in intact animals and animals that have neurological injury or disease. Thus, the aims of the current study were to define the somatotopy of trunk S1 and trunk M1 and examine sensorimotor integration of trunk cortex. First, to examine the internal organization of trunk S1, electrophysiological mapping was performed at the spinal level to identify thoracic dermatomes and their corresponding representation in S1. Similarly, intracortical microstimulation (ICMS) was used to examine the extent and internal organization of trunk M1. Then, sensorimotor integration was assessed by examining somatosensory evoked potentials across broad regions of sensorimotor cortex and retrograde tracing was performed to understand the source of somatosensory input to trunk M1. Finally, to understand the functional role of sensorimotor integration, single neuron activity was recorded from trunk S1 and M1 in response to unexpected postural perturbations while animals stood on a tilting platform. Results from mapping studies reveal an important somatotopic organization within both the trunk S1 and M1 cortices. Furthermore, there is extensive sensorimotor integration between trunk and hindlimb

82

83

84

85

86

87

88

89

90

91

92

93

94

95

96

97

98

99

100

101

102

103

systems, compared to the relatively weak integration within trunk and between trunk and forelimb cortices. Evidence from response latency and tracing studies suggest that this trunk/hindlimb sensorimotor integration is mediated predominately by thalamo-cortical projections. Importantly, this integration of hindlimb somatosensory information with trunk M1 is activated during postural adjustments to allow the animal to stabilize the trunk and maintain balance. These insights into trunk sensorimotor organization enhance our understanding of how information is processed during postural control and thereby inform the development of effective rehabilitative strategies after spinal cord injury.

#### **Materials and Methods**

#### **Subjects**

One hundred and six adult, female Sprague Dawley rats (225-250 g; Envigo) were maintained on a 12/12-hour light/dark cycle with ad libitum food and water. Fifteen animals were used to map the representation of each thoracic dermatome at the spinal level, 40 animals were used to map the internal representation of trunk S1, 21 animals were used to examine the movement representation of trunk M1, 14 animals were used to examine the integration of somatosensory information within and between sensory and motor cortices, five animals were used for anatomical tracing, and 11 animals were used to study sensorimotor integration relevant for postural control.

For all anesthetized experiments, animals were secured on a stereotaxic frame (Neurostar, Sindelfingen, Germany) and body temperature was maintained at 37°C using a temperature-controlled heating pad (FHC Inc., Bowdoin, ME). In addition, heart rate, SpO2, and anesthetic state (whisking/toe pinch reflex/corneal reflex) were constantly monitored. All experimental

procedures were approved by UC Davis or Drexel University IACUCs and followed NIH guidelines.

#### Body grid system to map receptive fields

To identify receptive fields (RFs) consistently across animals, a standardized grid was outlined on each animal's dorsal trunk (Blumenthal et al. 2021). The dorsal trunk was shaved and a grid of 128 equally spaced squares was drawn indelibly. The grid spanned from the skull's base, parallel to the intertragic notch of the ear, to the tail's base (16 grids in the rostrocaudal orientation), and from the dorsal trunk's midline to its lateral aspect at the base of the limbs on each side of the animal (8 grids in the mediolateral orientation; Figure 1A). Each grid square was approximately 1 cm<sup>2</sup> and was consistent across animals due to the similarity of both size and weight. In addition, a photograph of the animal with the drawn grid was taken to assist in defining RFs during S1 mapping experiments (Supplemental Figure 2).

### **Mapping thoracic dermatomes**

Animals were anesthetized with urethane (1.5 g/kg, IP) and maintained at Stage III-3 anesthesia (Friedberg et al. 1999). An incision was made along the midline of the trunk and axial musculature was separated from the vertebral column to expose the thoracic vertebrae. The spinous processes, lamina, and transverse processes of the selected thoracic vertebrae were carefully removed to access the dorsal root ganglion (DRG) on one side of the body. The animal's spinal column was secured in place by attaching locking forceps to the transverse process rostral to the T1 vertebrae and caudal to the T13 vertebrae. A single high-impedance (4-10 M $\Omega$ ) tungsten microelectrode (FHC Inc., Bowdoin, ME) was attached to the stereotaxic manipulator and a ground wire was placed in contact with the body cavity. The electrode was

positioned over a single DRG and lowered slowly until a single cell was identified. The neuronal signal (digitized at 40 kHz) was amplified (20000x), band pass filtered (150 - 8000 Hz; Plexon Inc., Dallas, TX) and monitored with an oscilloscope and through audio speakers. The cell's receptive field was then identified using light tactile stimulation (Chapin and Lin 1984; Chapin 1986). First, the dorsal cutaneous surface of the animal was tapped with a cotton brush, both within and outside the body grid to gain insight of the neuron's RF. If the RF was located within the trunk body grid, it was then mapped with a 0.25 body grid square resolution by applying light tactile stimulation to the cutaneous surface using a wooden probe (4 mm diameter). If the RF was found outside the grid, it was not included in the mapping of thoracic dermatomes. When mapping of that neuron's RF was complete, the electrode was lowered at least 50 μm dorsoventral (DV) before another cell was identified to ensure that the same cell was not mapped twice. This process was repeated until the electrode punctured through the entire DRG. Each DRG was sampled at least three times, so as to cover the DRG's rostrocaudal extent (Wessels et al. 1994). A trunk dermatome was defined as the union of all trunk grid locations on the skin that were found to be responsive to at least one cell in the respective DRG. The width of a dermatome was defined as the number of trunk grid locations within its rostrocaudal extent. Center position of a dermatome was defined as the center of this rostrocaudal extent. Dermatomal overlap was defined between two adjacent dermatomes as the distance between the rostral extent of the more caudal dermatome and the caudal extent of the more rostral dermatome.

#### Mapping trunk sensory cortex

149

150

151

152

153

154

155

156

157

158

159

160

161

162

163

164

165

166

167

168

169

170

171

Animals were anesthetized with urethane (1.5 g/kg, IP) and maintained at Stage III-3 anesthesia (Friedberg et al. 1999). A craniotomy was performed on the right hemisphere to expose hindlimb

S1 (HLS1), trunk S1 (TrS1), and parts of forelimb S1 (FLS1; Chapin and Lin 1984; Leergaard et al. 2004). Based on a pilot study (n = 3), 80 predefined cortical locations relative to Bregma were chosen. They extended from -2.0 mm to -3.8 mm rostrocaudal (RC) with a resolution of 0.2 mm, and from 2.0 mm to 3.75 mm mediolateral (ML) with a resolution of 0.25 mm between locations. At each location, the electrode was slowly lowered into the brain, up to a depth of -2.0 mm DV, while light tactile stimulation was applied to the cutaneous surface of the trunk. If a neuron was responsive, the neuron's receptive field was categorized into either trunk, ventral trunk, head/face, forelimb, hindlimb, tail, or a combination of body parts. If the RF included the trunk, the RF was further analyzed relative to the body grid with a 1.0 body grid square resolution and calculated separately for the supragranular, granular, and infragranular layers. A somatotopic map of the trunk and surrounding somatosensory cortices was constructed. At each cortical location, the proportion of cells that responded to each body part was investigated. A body part was assigned to a cortical location if at least 25% of the neurons in that location were responsive to that body part. If there were multiple body parts that meet the criterion, the body part with the highest proportion of responsive neurons was assigned (Figure 2B). To locate the cortical representation of the thoracic dermatomes within TrS1, all cells that had RF centers within trunk were used. For a given cortical location, the rostrocaudal positions of the RF centers on the body grid from all cells of that location were averaged. The dermatome with the closest center position to the average cortical RF position defined the corresponding dermatome of that cortical location. Cortical locations that represented the same dermatome were grouped to generate the representation of thoracic dermatomes in the cortex. All RFs belonging to the same dermatome representation were used to calculate the amount of overlap between the neighboring dermatome representations. To analyze the size and extent of trunk RFs, only

172

173

174

175

176

177

178

179

180

181

182

183

184

185

186

187

188

189

190

191

192

193

neurons that were completely contained within the borders of the trunk grid were used. Average RF size was calculated by averaging the number of responsive body grid squares for all cells.

#### Local field potential recording in response to peripheral electrical stimulation

195

196

197

198

199

200

201

202

203

204

205

206

207

208

209

210

211

212

213

214

215

216

217

Electrical stimulation was chosen to compare the S1 and M1 responses to stimulation across the hindlimb, forelimb, and trunk. First, bipolar electrodes placed in the hairy skin of the hindlimb, forelimb, and trunk, were used to activate afferents between the two poles of the electrode. Second, to ensure fair comparisons across stimulus locations, the response of HLS1, FLS1 and TrS1 to stimulation of their RF centers was titrated to produce similar magnitudes of response across the three sensory cortices. This would be difficult to accomplish with other stimulation modalities. Although mixing of tactile and proprioceptive afferent activation cannot be ruled out, a low intensity stimulus (0.5 mA) was used to predominantly activate tactile receptors between the two poles of the electrode, while a high intensity stimulus (5.0 mA) was used to elicit muscle twitches and slight movements that further activate proprioceptive afferents and nociceptive afferents (Lilja et al. 2006; Yagüe et al. 2014). This higher amplitude stimulus was necessary to identify sensory responses in trunk M1. Specifically, bipolar stimulating electrodes were inserted subcutaneously into the dorsal hairy skin at four locations: hindlimb (HL), forelimb (FL), T4-T5 dermatome of the upper trunk (UT), and T9 dermatome of the mid trunk (MT; approximately the midpoint of the trunk between the FL and HL), contralateral to the recording location (Figure 3A, Supplemental Figure 2A). For the trunk locations, the bipolar electrodes were placed approximately 5 mm apart from each other and approximately 20 mm from the midline of the animal (approximately halfway between the midline and the grid line border of the ventral trunk). Electrical stimulation, consisting of 100 pulses (1 ms duration) was delivered every 2 s at varying stimulation intensities (see Results).

To record local field potentials, animals were anesthetized with urethane (1.5 g/kg, IP). A craniotomy was performed on the right hemisphere to expose the sensory and motor cortices. A 32-channel, four shank recording electrode array (A4x8-5mm-200-400-177; NeuroNexus, Ann Arbor, MI) was positioned over the fixed locations either spanning M1 (-3.2 to 1.2 mm RC, 1.25 mm ML), TrS1 (-3.4 mm to -2.2 mm RC, 3 mm ML), HLS1 (-1 mm to -2.2 mm RC, 2.5 mm ML), or FLS1 (0.5 mm to -0.7 mm RC, 3.5 mm ML). The array was lowered perpendicularly into the cortex to a depth of 1.8 mm where it was fixed in place. The extracellular local field potential (LFP) was acquired simultaneously from all 32 channels (Intan Technologies, Los Angeles, CA), digitized at 20 kHz, amplified (192x) and band pass filtered (0.1 Hz – 7.5 kHz). To ensure fair comparisons between the stimulation responses of different locations on the body, the responses of each region to stimulation of their RF centers were compared (RF center identified using light tactile stimulation, see above). A high pass filter of 5 Hz was used to mitigate slow wave activity that developed under urethane anesthesia (Clement et al. 2008; Humanes-Valera et al. 2013) in the cortical LFP. A window of 1 s centered on the stimulation time was extracted from the high pass filtered LFP data (5 Hz, Butterworth order 2, zero-lag) of each recording site. The data in that window was then averaged across stimulation trials to obtain the somatosensory evoked potential (SEP). A representative channel from the supragranular (400 µm DV), granular (800 µm DV), and infragranular (1200 µm DV) cortex was selected for further analysis (Supplemental Figure 3). For each layer, the SEP was considered responsive if the amplitude exceeded the mean background activity by three standard deviations. SEP amplitude was evaluated as the absolute value of the first negative peak of the SEP, normalized to the background activity. Peak latency of the SEPs was calculated as the time of the SEP peak amplitude post stimulus. Only responsive SEPs with a latency less than or equal

218

219

220

221

222

223

224

225

226

227

228

229

230

231

232

233

234

235

236

237

238

239

to 50 ms were considered for further analysis to capture the short latency response. In addition, the LFP from each electrode was filtered (300-8000 Hz) and single neurons were discriminated using PCA and visual inspection using Offline Sorter (Plexon Inc., Dallas, TX).

Single neuron spike times were used to construct peri-stimulus time histograms (PSTH) to determine the magnitude of the response of a neuron to the peripheral electric stimulation using previously published methods (Foffani and Moxon 2004; Tutunculer et al. 2006; Foffani et al. 2008; Kao et al. 2009; Manohar et al. 2017). The PSTH consisted of spike counts within 5 ms bins averaged across 100 trials within a window of 100 ms from the time of stimulus (Figure 3E). A neuron was considered responsive if at least two consecutive bins in the PSTH exceeded three standard deviations above the background window. Response magnitude and the proportion of responsive neurons were quantified from neurons recorded across all layers in S1.

#### Mapping trunk motor cortex

The representation of trunk primary motor cortex (TrM1) was examined by analyzing evoked movement and EMG activity in response to stimulation of infragranular neurons in M1 using previously published methods (Ganzer et al. 2016). Animals were anesthetized with ketamine (63 mg/kg, IP), xylazine (6 mg/kg, IP) and acepromazine (0.05 mg/kg, IP) and administered dexamethasone (5 mg/kg, IM) to control blood pressure and brain swelling. Supplemental doses of ketamine (20 mg/kg, IP) were administered when necessary, to maintain the animal at light Stage III-2 anesthesia throughout the entire mapping procedure (Friedberg et al. 1999; Tandon et al. 2008). Animals were placed in a stereotaxic frame in a prone position such that the limbs could hang freely. Eight bipolar intramuscular electromyogram (EMG) electrodes (stainless steel, 7 strands, AM-Systems Inc., Sequim, WA) were implanted on dorsal (longissimus) and ventral (external oblique) trunk muscles at the upper thoracic (T4-T5), mid thoracic (T9-T10)

and lower thoracic (T12-T13) levels. One EMG electrode was implanted in each of the contralateral shoulder/trunk (spinous trapezius), contralateral forelimb (forelimb bicep), contralateral hindlimb hip (gluteus maximus) and hindlimb ankle (tibialis anterior; Figure 4A). Based on previous studies on rats (Neafsey et al. 1986; Oza and Giszter 2015; Ganzer et al. 2016), a craniotomy exposed the medial post bregma area and the caudal forelimb area (1 mm to -3.5 mm RC, 1 mm to 3 mm ML). Similar to the somatosensory mapping procedure, 88 predefined cortical locations were chosen spanning the craniotomy. The medial portion (<1 mm) could not be mapped reliably due to methodological constraints related to the high density of blood vessels in this region that limits access to the cortex. Previously, (Donoghue and Wise 1982) reported that responses could not be evoked from these medial regions. This region, often referred to as medial agranular cortex or M2, is cytoarchitecturally different from M1. A low impedance glass insulated tungsten electrode (100-500 k $\Omega$ ; FHC Inc., Bowdoin, ME) attached to a stereotaxic manipulator was inserted into one of the 88 predefined cortical locations. In order to assess microstimulation waveform quality, the voltage drop across a 10 k $\Omega$ resistor interposed in series between animal ground and the isolated current pulse stimulator (Model 2100, A-M systems, Sequim, WA) was monitored with an oscilloscope. At each M1 location, the electrode was lowered to the infragranular layer (1.5 mm DV) and a long train ICMS was applied (Young et al. 2011; Griffin et al. 2014), consisting of 0.2 ms cathodal leading bipolar current pulses (10 to 100 µA) delivered at 333 Hz for 300 ms. This long train was used to evoke muscle synergies (overlapping representations/coactivation of segmental muscle groups) that represent complex movement repertoires. Pilot experiments with 60 ms stimulus trains showed that stimulus-evoked movement represented short, truncated movements and muscle twitches, while 300 ms pulse trains often elicited a variety of movements ranging from simple

264

265

266

267

268

269

270

271

272

273

274

275

276

277

278

279

280

281

282

283

284

285

(muscle contraction across a single joint) to more complex movements that represented the coactivation of muscles across different segmental levels of trunk / across multiple joints consistent with other studies (Graziano et al. 2002; Ramanathan et al. 2006; Giszter et al. 2008; Brown and Teskey 2014; Overduin et al. 2014; Baldwin et al. 2017; Halley et al. 2020). The stimulation current was gradually increased in steps of 10 µA until a reliable movement or EMG response was found. EMG signals and current stimulus times were sent to a data acquisition system (Intan Technologies, Los Angeles, CA). EMG was sampled at 5 kHz, zero-lag band pass filtered (40-400 Hz) and rectified. An EMG envelope was obtained by further filtering the data (zero-lag Butterworth low pass filter, 20 Hz, 5th order). The EMG envelope was normalized to its peak value to account for changes in EMG response due to electrode placement, impedance mismatch, signal to noise ratio, and muscle size (Kargo and Nitz 2003). Motor evoked potentials (MEPs) were then obtained by averaging the processed EMG over a time window of 1 s centered on the current stimulus timestamps. If the amplitude of a MEP exceeded the background EMG activity by five standard deviations, it was considered a responsive EMG. The minimum current required for eliciting a movement/EMG response was defined as the threshold current for that cortical location. Once a reliable threshold current was found, the current was increased to 100 uA (suprathreshold), and the movement and EMG responses were recorded. A minimum of five separate stimulations were performed in every cortical location. If no movement or EMG response was evoked with the 100 µA current, the cortical location was determined nonresponsive. If there were more than three consecutive non-responsive locations, the closest responsive location was rechecked to identify the limits of motor cortex. A combination of visual observation of movements and reponsive EMG locations were used to classify cortical locations

287

288

289

290

291

292

293

294

295

296

297

298

299

300

301

302

303

304

305

306

307

308

into movement types (Table 1). Recruitment of trunk musculature via stimulation of the TrM1 was examined based on EMG response. Trunk musculature responses were classified into different categories based on the location of responsive trunk EMG along the thoracic level at both threshold and suprathreshold currents (Table 2, Figure 5A). At threshold, the proportion of responsive EMG was compared across thoracic levels.

The muscle responses (muscle identification and movement type) associated with the stimulation of each cortical location were used to calculate a responsiveness score (Girgis et al. 2007; Ganzer et al. 2016). For each movement type (or trunk musculature type), the proportion of responses in each location was determined and transformed to a score as follows: ranges of 0, 1-33%, 34-66%, and 67-100% received a score of 0, 1, 2, or 3, respectively. For example, if only one animal responded to cortical stimulation at a cortical location out of five animals that were stimulated at that spot, the occurrence rate would be 0.2 or a score of 1. A score of 0 meant that no movement and no EMG response were recorded and a score of 3 meant that the muscle movement (or EMG response) was elicited for 67 -100% of the cortical stimulation. The average responsiveness score for a specific movement type and/or EMG response was calculated by averaging the score across cortical locations. To control for the fact that not every cortical location was sampled equally, a responsiveness score was only included in the analysis if there were at least five penetrations in a given location.

#### Retrograde tracing

To gain insight into the regions of the brain that project sensory input to TrM1, a tracing study was performed. Results from the ICMS mapping showed that only a small location in the brain exclusively activated trunk musculature and most of TrM1 included coactivation with other body parts. However, the location of this exclusively trunk area was variable across animals. Although

a ICMS study prior to tracer injection could have located this exclusively trunk region in each animal, this would have severely damaged the tissue and made the tracing unreliable. Therefore, the tracer was injected into the most likely location that exclusively activated trunk musculature. Animals were anesthetized with ketamine (63 mg/kg, IP), xylazine (6 mg/kg, IP), and acepromazine (0.05 mg/kg, IP). A craniotomy was made over TrM1 (-0.5 mm RC, 1.25 mm ML, 1.65 mm DV) and 300 nL of 10% fluorescent microbeads (Lumafluor Inc., Naples, FL.; Figure 4D, Figure 7A) were injected with a Hamilton syringe (tip diameter: 0.1 mm). Three days after the injection, animals were perfused with saline followed by 4% PFA and brains were removed. 50 µm coronal sections were mounted under Permount (Fischer Chemical, Geel, Belgium) on microscope slides. Brain slices were then imaged using a wide field microscope (5x/.012 numerical aperture; ZEISS, Oberkochen, Germany) and cell counting was performed using ImageJ (National Institutes of Health, Bethesda, MD). Images were transformed to an 8-bit grey scale image and thresholding was done to minimize artifacts caused by autofluorescence. Automated cell counting (minimum size: 100 pixels<sup>2</sup>) was conducted in the region of interest (ROI). The different ROIs, corresponding to the different somatosensory cortices were identified based on electrophysiological sensory mapping data (Figure 2B). For locations outside of TrS1, ROIs for HLS1 and FLS1 were identified based on (Leergaard et al. 2004). Only ipsilateral projections were identified. The location of thalamic nuclei was identified by superimposing our images on to the rat brain atlas (Paxinos & Watson 2007).

#### Postural control task (tilt task)

333

334

335

336

337

338

339

340

341

342

343

344

345

346

347

348

349

350

351

352

353

354

355

The tilt task was used to understand sensorimotor integration in the cortex relevant for postural control. Microwire arrays (32 channel each [8\*4], 250 µm resolution, Microprobes, Gaithersburg, MD) were implanted bilaterally in the infragranular layer of the cortex, spanning TrS1, HLS1, and FLS1 on the left hemisphere and TrM1 and on the right hemisphere. For chronic microwire implantation refer to previously published methods (Foffani et al. 2008; Manohar et al. 2012; Bridges et al. 2018). Single neuron activity was recorded from the different cortices in response to sudden unexpected postural perturbation in the lateral plane. Four different tilt types were tested, two to the left and two to the right. For each direction, there was a slow speed (max speed: 26.2°/s; duration to final amplitude: 0.9 s) and a fast speed (max speed: 76.5°/s; duration to final amplitude: 0.5 s). The final angle for all tilt types had the same final amplitude of 16.5° (Figure 8A). The task was adapted from (Bridges et al. 2018) and engaged the cortex bilaterally. Based on the mapping results, the recording electrodes in M1 were grouped based on the region of the body they most likely activated. Electrodes spanning caudal TrM1 (-1 mm to -2 mm RC, 1.25 mm to 1.5 mm ML; Figure 5F) preferentially activated lower thoracic trunk musculature and were defined as lower thoracic trunk primary motor cortex (LTM1). Electrodes rostral to LTM1 (0 mm to -0.75 mm RC, 1.25 mm to 2.0 mm ML) were more likely to control upper thoracic muscles and were labelled upper trunk primary motor cortex (UTM1). Regions lateral to LTM1 (-1 mm to -2 mm RC, 1.75 mm to 2 mm ML) preferentially controlled hindlimb musculature and were defined as hindlimb primary motor cortex (HLM1). Similarly, for each of the electrodes spanning the somatosensory cortex (left hemisphere), the corresponding RF center (i.e., stimulus location that produced the largest SEP amplitude) was identified in response to peripheral electric stimulation (0.5 mA, tactile) of the different body parts (forelimb, hindlimb, upper, mid, and lower trunk). The electrode was then labelled as recording from FLS1, HLS1, UTS1, MTS1 or LTS1 based on the RF center. Responsiveness in the different cortices was calculated as the proportion of responsive neurons to at least one tilt type. A neuron was considered responsive to a tilt if the neuronal activity in the

356

357

358

359

360

361

362

363

364

365

366

367

368

369

370

371

372

373

374

375

376

377

response window (400 ms from start of tilt) was significantly different from the background and there were at least five consecutive bins (bin size 5 ms) in the response window that exceed the background activity by two standard deviations. The magnitude of response (spikes per second) was defined as the change in the average neuronal firing rate from the background (average firing rate in response window – average background firing rate). Shannon's mutual information was used to quantify the information about the tilt type provided by the neuronal response of each single neuron within the region (Liu et al. 2017). If a neuronal response and a tilt type are completely independent from each other, mutual information is 0 bits, and if they are perfectly correlated, the mutual information is defined by the entropy of the stimulus (tilt type) and is 2.0 bits (i.e.,  $log_2(4)$ , n = 4 tilt types) of information.

#### **Statistical Analysis**

Statistical analyses were conducted using GraphPad Prism 9.0.1. Continuous variables with a normal distribution are reported as mean + standard error; variables with a non-normal distribution are reported as median (interquartile range). Differences between two independent groups were assessed using an Independent Samples t-test for normally distributed data, or a Mann-Whitney U test for non-normal data. Differences between three or more independent groups were assessed using analysis of variance (ANOVA) with a Tukey post-hoc test for normally distributed data, or a Kruskal-Wallis test with a Dunn's post-hoc test for non-normal data. Frequencies were compared using Pearson  $\chi^2$  or Fisher's exact test. A value of p < 0.05 was considered significant and significant group effects were subjected to Tukey's honest significant difference post-hoc test. p < 0.05 is denoted by \*, p < 0.01 by \*\*\*, p < 0.001 by \*\*\*\*, and p < 0.0001 by \*\*\*\*.

401 Results

To study how trunk somatosensory information is represented in the brain, it is important to understand how this somatosensory information is first represented at the spinal level. While the upper and lower thoracic dermatomes were previously mapped (Lombard et al. 1979; Smith 1986; Takahashi et al. 1994; Wessels et al. 1994), the mid thoracic dermatomes have not been mapped extensively in the rat, nor is the representation of these dermatomes in the cortex known. To this end, we recorded single neuron activity from DRGs at the thoracic level (T1-T13) and mapped the thoracic dermatomes (Figure 1A). An average of 6 +/- 3 DRGs were recorded per animal (n = 15) for a total of 86 recorded dermatomes. The thoracic dermatomes were rectangular bands with overlapping receptive fields that extended from the dorsal midline to the midline on the ventral side of the trunk. The T1-T3 dermatomes had receptive fields that extended into the forelimb, while the receptive fields of the remaining thoracic dermatomes were limited to the trunk (Figure 1B). The width of the thoracic dermatomes remained constant in the rostrocaudal direction along the body (One-way Repeated Measures ANOVA, F(12, 59) = 1.41, p = 0.44; Figure 1C), consistent with studies performed on cats (Kuhn 1953; Hekmatpanah 1961), sheep (Kirk 1968), and monkeys (Sherrington 1892; Kirk and Denny-Brown 1970). However, the amount of overlap between adjacent dermatomes decreased significantly from rostral to caudal (One-way Repeated Measures ANOVA, F [11, 44] = 2.52, p < 0.05; Figure 1D). This decrease in overlap was due to a shift in the average center position of adjacent dermatomes (One-way ANOVA, F[2, 61] = 7.73, p < 0.001; Figure 1E). Tukey's post-hoc test revealed a significant increase in the average positional shift distance between adjacent dermatomes in both the mid (T5-T9; p < 0.05) and lower (T9-T13; p < 0.001) trunk regions when compared to upper

Dermatomes of upper thoracic DRGs overlap more than those of lower thoracic DRGs

402

403

404

405

406

407

408

409

410

411

412

413

414

415

416

417

418

419

420

421

422

# trunk dermatomes (T1-T5). Therefore, rostral DRGs appeared to overlap more with neighboring dermatomes than caudal DRGs.

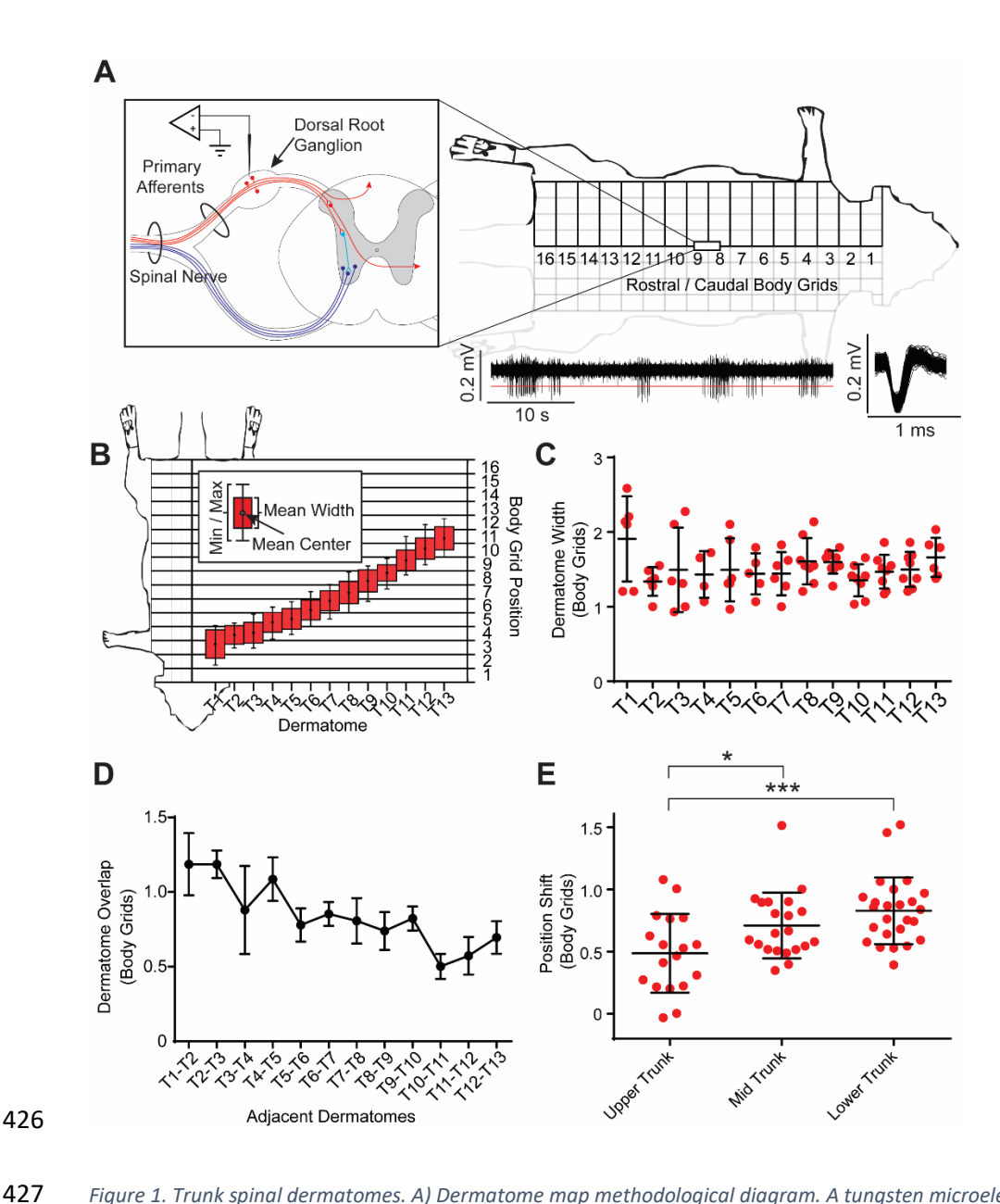


Figure 1. Trunk spinal dermatomes. A) Dermatome map methodological diagram. A tungsten microelectrode was inserted into an average of 6 +/- 3 thoracic level dorsal root ganglions (DRGs) per animal (N = 15), to record from primary afferent cell bodies and identify their receptive fields (N = 86). An example of a continuous neural trace is shown in the bottom right. B) Average dermatome width in body grid units (each grid unit is approximately 1 cm²) and center position plotted along the rostrocaudal axis of the body. The error bar represents the most rostral and the most caudal body grid positions of each dermatome across all animals. C) Average dermatome width is similar throughout the rostrocaudal axis. D) Average overlap between adjacent dermatomes showed a shift in the rostrocaudal axis. E) Average distance in between neighboring dermatomes within the upper (T1-T5), mid (T5-T9), and lower (T9-T13) thoracic dermatomes showed a shift in the rostrocaudal axis, with a significant difference for the average distance in between neighboring dermatomes between upper trunk and mid trunk and between upper trunk and lower trunk.

#### Sensory information from mid and lower trunk most likely to overlap within S1

437

438

439

440

441

442

443

444

445

446

447

448

449

450

451

452

453

454

455

456

457

458

459

A somatotopic map of TrS1 and surrounding somatosensory cortices was constructed using single unit cortical mapping data as well as information from the dermatomes. In each cortical location, the proportion of cells responding to each body part was calculated (Figure 2A). An average of 9  $\pm$  3 cortical locations were sampled per animal (N = 40 animals), with an average of 8 +/- 3 single neurons sampled per location. In total, more than 2900 neurons were recorded. TrS1 was determined to be located along the caudal edge of FLS1 and HLS1, consistent with previous studies in rats (Chapin and Lin 1984; Xerri et al. 1994; Seelke et al. 2012). The representation of the neck was most lateral, with the tail representation most medial (Figure 2B). Dorsal TrS1 was located more caudal to ventral TrS1. The ventral TrS1, consistent with previous studies (Chapin and Lin 1984; Xerri et al. 1994; Seelke et al. 2012), was nestled between the FLS1 (lateral) and the HLS1 (medial), and rostral to midthoracic (T6-T9) trunk representations, overlapping with the genital cortex described in previous studies (Lenschow and Brecht 2018). The full rostral extent of ventral trunk was not mapped. Nonetheless, these results show that the trunk representation is larger than previously reported (Hall and Lindholm 1974; Gioanni and Lamarche 1985; Ganzer et al. 2016). Within the trunk representation, the thoracic dermatomes were represented from T1, laterally, to T13, medially, consistent with a study in humans (Itomi et al. 2000). As might be expected, there was extensive overlap of the cortical representation of neighboring thoracic dermatomes (Figure 2C). The rostrocaudal dimension of the dorsal trunk body was represented along the mediolateral axis of the cortex, with rostral trunk body represented laterally in the TrS1 (Figure 2C1). The mediolateral dimension of the dorsal trunk body was represented along the rostrocaudal axis of the cortex, with the most lateral part of dorsal trunk body represented rostrally in the cortex, just

caudal to the ventral trunk representation (Figure 2C2). Unlike other sensory systems, such as whisker and limbs that tend to have RF size differences across layers (Chapin 1986), the RF size of neurons in TrS1 were similar across layers (N = 482) (One-way ANOVA, F [2, 479] = 1.45, p = 0.23; Figure 2D1). However, the RF size of trunk neurons did differ across the different regions of the TrS1 (N = 437) (One-way ANOVA, F [2, 434] = 19.71, p < 0.0001; Figure 2D2) with upper trunk neurons having smaller RF size compared to both mid and lower trunk neurons (5.7 +/- 3.7, 8.0 +/- 3.8, 9.0 +/- 5.0 body grids or cm², respectively; Tukey's post-hoc test, p < 0.0001; Figure 2D2-2D3). This RF size analysis suggests that somatosensory information ascending from the thalamus is spread across large parts of TrS1 early, immediately upon arrival in layer IV, with more overlap between mid and lower trunk sensory information than that of upper trunk. This is consistent with RF sizes observed in forepaw somatosensory cortex that varied from relatively small in the digits to larger in the limb (Foffani et al. 2008).

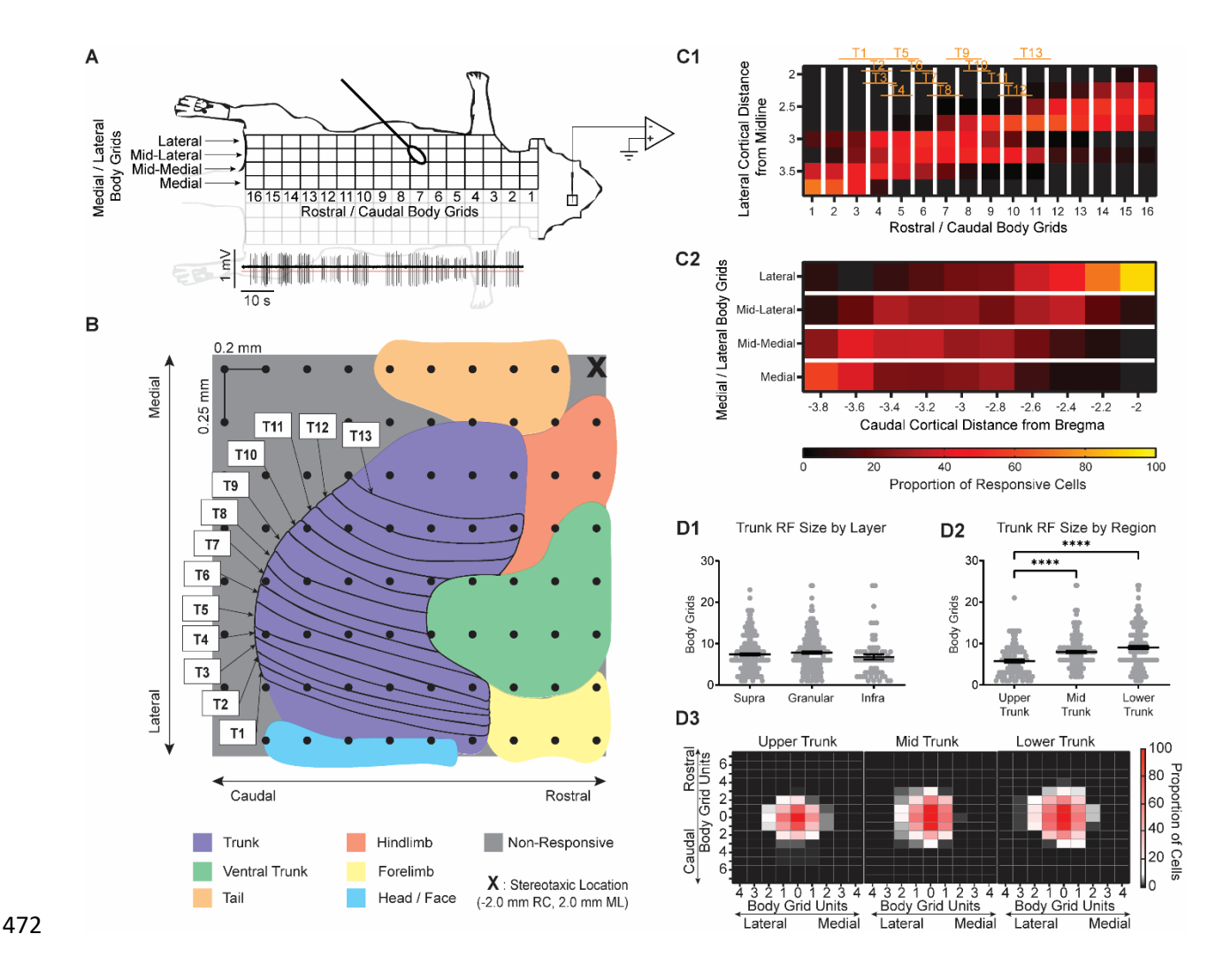


Figure 2. Relationship of trunk S1 organization in relationship to spinal dermatomes. A) Sensory map methodological diagram. A tunasten microelectrode was inserted into several locations within and around trunk S1. Single units were isolated, and their receptive fields were determined. B) Cortical representation of the thoracic dermatomes. The map shows the average cortical representations across cortical layers. Based on a pilot study (N = 3), 80 predefined cortical locations were chosen (black dots). They extended from -2.0 mm to -3.8 mm rostrocaudal (RC) from bregma with a resolution of 0.2 mm, and from -2.0 mm to -3.75 mm mediolateral (ML) with a resolution of 0.25 mm between locations, in order to optimally map the dorsal trunk area. 2920 neurons were recorded across all animals (N = 40) to construct the map. C1) Proportion of cells identified in the mediolateral cortical axis across all animals, associated with body grid rows, to light tactile stimulation of which the cortical cells responded. A higher proportion of rostral trunk RFs were found at lateral cortical coordinates, while a higher proportion of caudal trunk RFs were found at medial cortical coordinates. The rostrocaudal extent of the thoracic dermatomes relative to the body grid rows are also displayed. C2) Proportion of cells identified in the rostrocaudal axis across all animals, associated with body grid columns, to light tactile stimulation of which the cortical cells responded. A higher proportion of lateral trunk RFs were found at rostral cortical coordinates, while a higher proportion of medial trunk RFs were found at caudal cortical coordinates. The color scale bar at the bottom is for both C1 and C2. D1) Trunk receptive field size (body grids units) (N = 482) of neurons in the supragranular, granular and infragranular layers are similar. D2) Receptive field size  $\frac{(N = 437)}{N}$  is significantly different for the upper, mid, and lower trunk S1 regions. D3) Receptive field centers are normalized to position (0, 0) and the proportion of cells responsive to the surrounding body grids are calculated and showed significant differences in size across trunk S1 regions (refer

#### Greater overlap of trunk S1 with hindlimb than forelimb S1

473

474 475

476

477

478

479

480 481

482

483

484

485

486

487

488

489

490

To understand the overlap between trunk, forelimb, and hindlimb somatosensory information, multichannel recordings were performed in TrS1, FLS1, and HLS1 in response to peripheral electrical stimulation of the mid trunk, forelimb, and hindlimb. To ensure fair comparison between the responses to the different stimulus locations on the body, the amplitudes of the SEP recorded from the granular layer at each cortical region in response to graded peripheral electric stimulation of each respective region (FL, HL, and MT) were compared (Figure 3A, Supplemental Figure 2B). As expected, there was a significant increase in the SEP amplitude associated with increases in stimulus current regardless of stimulus location (Two-way Repeated Measures ANOVA, F [3, 70] = 15.47, p < 0.0001; Figure 3A). However, across stimulus location, the SEP amplitudes were similar (Two-way Repeated Measures ANOVA, F[2, 70] =1.62, p = 0.21; Figure 3A), suggesting that the stimulus at each location activated the homologous cortical region similarly and that comparisons could be made between responses recorded from different brain regions to stimulation of the same location on the body. To understand the overlap of trunk somatosensory information across S1, the amplitude of the SEP response to mid trunk stimulation recorded from FLS1 was compared to the SEP response recorded from HLS1. The SEP amplitudes recorded from FLS1 and HLS1 in response to low intensity trunk stimulation (0.5 mA) were similar (Independent Samples t-test, t [6] = 0.29, p = 0.77), suggesting trunk somatosensory information overlaps with both FLS1 and HLS1. However, when the stimulation amplitude was increased to produce twitching of the underlying muscle and further activate proprioceptive receptors (5.0 mA), the response in HLS1 was significantly greater than that recorded from FLS1 (Independent Samples t-test, t [8] = 2.30, p = 0.05; Figure 3B, Supplemental Figure 2C-2D), suggesting differences in the overlap of trunk somatosensory information in HLS1 compared to FLS1.

492

493

494

495

496

497

498

499

500

501

502

503

504

505

506

507

508

509

510

511

512

513

Next, within TrS1, the relationship between inputs to layer IV cells (SEP amplitude) and outputs of TrS1 neurons (single neuron firing rate or proportion of responding neurons) in response to low and high intensity mid trunk stimuli were examined to assess the effectiveness of the information transfer from input to output (Figure 3C). As noted above, SEP amplitude to high intensity mid trunk stimulation was significantly greater than the response to low intensity stimulation (Independent Samples t-test, t [14] = 4.76, p < 0.001). This increase in input results in a greater magnitude of the response (spikes per stimulus) to high intensity stimuli (Independent Samples t-test, t [65] = 2.59, p < 0.05; Figure 3C) without a change in the proportion of responsive neurons ( $\chi^2$  [1, N = 55] = 0.46, p = 0.50), suggesting the same cells are responding to low intensity stimuli as those that respond to high intensity. Next, the contribution of high intensity forelimb and hindlimb stimulation to the response in TrS1 was examined. The SEP amplitude in TrS1 to forelimb stimulation was similar to that of hindlimb stimulation (Independent Samples t-test, t [8] = 0.36, p = 0.73). However, the proportion of neurons in TrS1 that responded to hindlimb stimulation was greater than the proportion responding to forelimb stimulation ( $\chi^2$  [1, N = 84] = 11.16, p < 0.001; Figure 3D), suggesting that the transfer of incoming somatosensory information to output is more effective for hindlimb than forelimb stimulation. In fact, too few cells responded to forelimb stimulation to allow any further analysis. To understand if the increased proportion of responsive TrS1 cells to hindlimb stimulation was potentially influenced by the proximity of these body or somatotopic regions, recordings were performed in upper TrS1 during stimulation to forelimb and hindlimb (5.0 mA; n = 3). No differences were found in SEP amplitude (Independent Samples t-test, t [4] = 0.09, p = 0.92) or the proportion of responsive cells ( $\chi^2$  [1, N = 107] = 2.95, p = 0.09) between stimuli conditions,

515

516

517

518

519

520

521

522

523

524

525

526

527

528

529

530

531

532

533

534

535

536

538 suggesting that proximity is likely not contributing to increased responsiveness (Supplemental 539 Figure 2E). 540 As expected, the response of TrS1 neurons to hindlimb stimulation was smaller than the response to MT stimulation (Independent Samples t-test, t [43] = 2.71, p < 0.01; Figure 3D-3E). These 541 results, taken together, suggest reciprocal flow of information between TrS1 and both FLS1 and 542 543 HLS1, with greater influence of trunk somatosensory information in HLS1 compared to FLS1 544 and greater influence of hindlimb somatosensory information in TrS1 compared to forelimb information. In the last section of this paper, we explore how this organization is used to encode 545 546 the cortical response to unexpected tilts in the lateral plane.

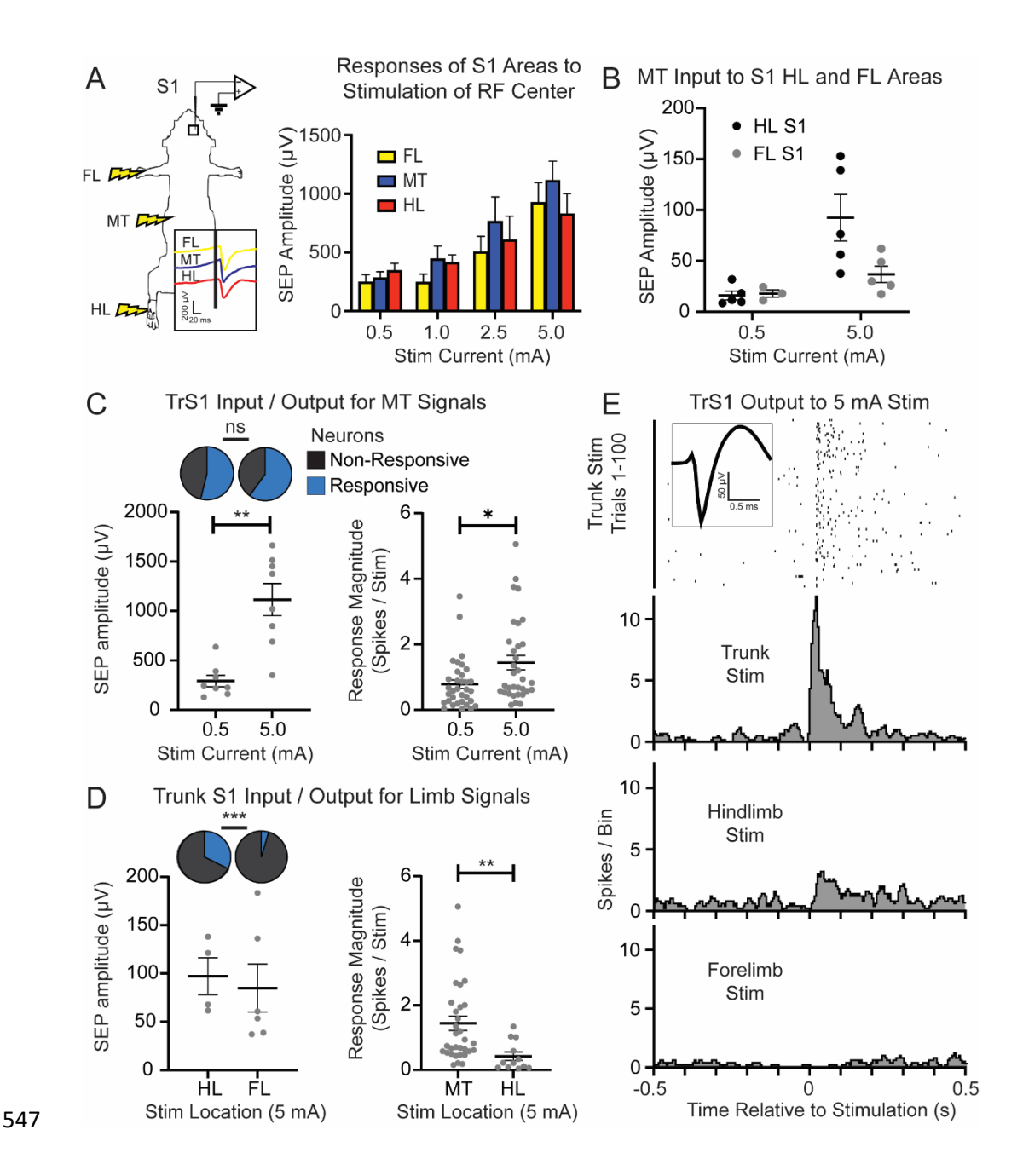


Figure 3. Somatosensory integration within trunk S1. A) Electric stimulation methodological diagram. Multichannel recordings were performed in the trunk, forelimb, and hindlimb S1 in response to peripheral electrical stimulation to the mid trunk (MT), forelimb (FL), and hindlimb (HL). The SEP from each cortical region recorded from the granular layer to graded peripheral electric stimulation (0.5 mA, 1.0 mA, 2.5 mA, 5.0 mA) of each respective region (FL [N = 5, 6, 7, 8], HL [N = 7, 6, 6, 7], MT [N = 9, 7, 6, 8]) was compared (also see Supplemental Figure 2). B) SEP amplitude in the forelimb S1 and hindlimb S1 in response to the low intensity (0.5 mA; FLS1 [N = 3], HLS1 [N = 5]) and the high (5.0 mA; FLS1 [N = 5], HLS1 [N = 5]) MT stimulation. C) The relationship between sensory inputs (SEP amplitude in the granular layer, left) (0.5mA N = 8; 5.0mA N = 8) and outputs (single neuron activity in all layers, right) (0.5mA N = 34; 5.0mA N = 33) in trunk S1 in response to low and high intensity MT stimuli. The inset on the top left represents the proportion of responsive cells for each stimulus. D) Bottom left: SEP amplitudes recorded from trunk S1 in response to high intensity HL (N = 4) and FL (N = 6) stimulation. Top left: Proportion of trunk S1 neurons responding to hindlimb or forelimb stimulation. Right: Trunk S1 response to MT (N = 33) and HL (N = 12) stimulation calculated within 100 ms from stimulus onset. E) Example PSTHs for trunk, HL, and FL stimulation (5.0 mA) in trunk S1, illustrating that trunk S1 activity is modulated more by hindlimb than forelimb.

## Coactivation of trunk musculature with hindlimb is more likely than coactivation with

#### forelimb musculature

561

562

563

564

565

566

567

568

569

570

571

572

573

574

575

576

577

578

579

580

581

582

583

To gain a better understanding of the trunk cortex, it was essential to examine the extent and organization within TrM1. The extent of TrM1 was mapped using ICMS and movement representations were examined by analyzing movement and EMG responses from trunk and limb musculature (Figure 4A). Each of the 88 cortical locations were sampled an average of 7 +/- 2 times, across 21 animals. Each animal contributed to the data with an average of 27 +/- 2 cortical locations per animal. The average threshold current was 51.3 +/- 23.4 mA. The areas of the cortex that most likely activated the trunk musculature were within 1.5 mm ML and 0.25 mm to -2.25 mm RC, relative to bregma (Figure 4B). This placed the rat TrM1 medial to FLM1 and HLM1 and just caudal to whisker M1. A much larger area than previously reported activated trunk by generally coactivating with other parts of the body, suggesting that this coactivation with forelimb and hindlimb motor cortex is functionally relevant. For each animal, the area that exclusively activated trunk musculature (ET) was quite small, and the location of ET was not consistent across animals. This suggests that there are likely to be few conditions under which trunk musculature is activated independently of the musculature of other parts of the body. In fact, it is possible to identify distinct coactivation zones between trunk and other parts of the body. The overall extent of the trunk coactivating with other parts of the body (Figure 4C) spanned -2.25 mm to 0.75 mm RC and 1 mm to 2.5 mm ML relative to bregma, which is much larger than previously reported (Gioanni and Lamarche 1985; Neafsey et al. 1986; Tandon et al. 2013; Frost et al. 2015; Oza and Giszter 2015; Ganzer et al. 2016). The area that exclusively activated trunk musculature (ET) within any given animal was restricted to within 1.5 mm lateral to midline (Figure 4D).

Despite this small area devoted to ET, coactivation of trunk with hindlimb musculature (HLT) was quite large (Figure 4E) and, not surprisingly, caudal to locations overlapping with forelimb (FLT; Figure 4F). In addition, consistent with an earlier study (Boyeson et al. 1991), in approximately half of the animals (45%), FL, HL, and trunk (synergistic trunk or FHT) coactivated in locations between the HLT and FLT representation (Figure 4G). In order to quantify and compare the different movement representations found within the trunk coactivation zone, responsiveness scores (Girgis et al. 2007; Ganzer et al. 2016) that represented the proportion of responses for each representation were compared. The responsiveness scores were different across coactivation zones (N = 54) (One-way ANOVA, F [7, 424] = 11.10, p < 0.001; Figure 4H). Importantly, the responsiveness score of HLT was significantly greater than FLT (Tukey's post-hoc test, p < 0.01), indicating that trunk coactivates more with hindlimbs across a larger region of cortex compared to forelimbs. Moreover, the responsiveness score of FLHL and FHT were very similar, suggesting that when forelimb and hindlimb coactivate, about half the time they coactivate with trunk. These results demonstrate that a large region of M1 is devoted to coactivating trunk musculature with musculature from different body parts, mainly hindlimb and less so with forelimb.

584

585

586

587

588

589

590

591

592

593

594

595

596

597

598

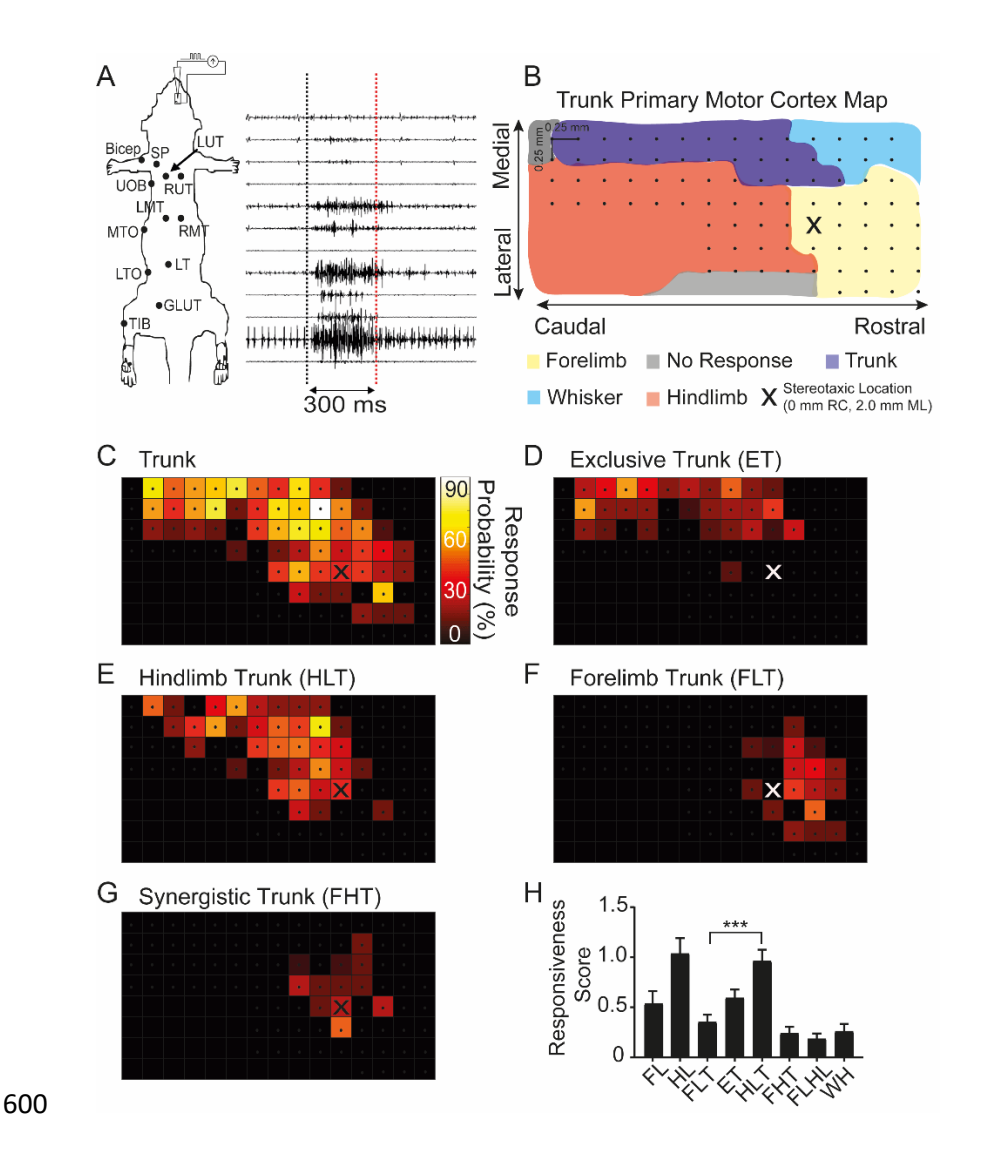


Figure 4. Coactivation of trunk musculature with forelimb and hindlimb. A) ICMS methodological diagram. Motor maps were obtained by intracortical current microsimulation (ICMS) in the infragranular layer of motor cortex. Evoked muscle activity was recorded through EMG electrodes implanted along the trunk, forelimb, and hindlimb musculature (Top to bottom: forelimb bicep [bicep], spinous trapezius [SP], left upper thoracic longissimus [LUT], right upper thoracic longissimus [RUT], upper external oblique [UOB], left mid thoracic longissimus [LMT], right mid thoracic longissimus [RMT], mid thoracic external oblique [MTO], lower thoracic longissimus [LT], lower thoracic external oblique [LTO], gluteus maximus [Glut], tibialis anterior [Tib]). Observed movement and evoked muscle activity at threshold current were used to determine movement representation. B) Topography of TrM1 is based on the most predominant response across animals. The dots refer to penetration locations sampled across animals. The X location refers to 0 mm RC, 2 mm ML, relative to bregma. C-G) Proportion of penetrations from which the following muscles were activated: (C) trunk, (D) trunk exclusively, (E) trunk and hindlimb, (F) trunk and forelimb, and (G) trunk and both forelimbs and hindlimbs. H) Average responsiveness score within trunk M1 (N = 54) was calculated for the different movement representations identified during mapping with ICMS (see Materials and Methods for explanation). FL (activation of forelimb only), HL (activation of hindlimb only), FLT (coactivation of only forelimb and trunk), FLHL (coactivation of only forelimb and hindlimb), WH (activation of whisker pad).

Movement type	Visual observation	EMG response
Forelimb (FL)	Isolated movement of forelimb (wrist or multi-joint)	Exclusive EMG response- FL muscle (FL bicep)
Hindlimb (HL)	Isolated movement of hindlimb (digits or multi-joint)	Exclusive EMG response- HL muscles (gluteus, tibialis)
Forelimb Trunk (FLT)	Proximal shoulder movement	Coactivation of FL muscle and Trunk /shoulder muscles
Exclusively Trunk (ET)	Isolated movement of thoracic girdle	Exclusive EMG response- Trunk muscles
Hindlimb Trunk (HLT)	Movement of hindlimb knee /ankle along with thoracic girdle	EMG response -Trunk muscles
Synergistic Trunk (FHT)	Forepaw and HL ankle dorsiflexion movements with trunk adduction	EMG response- Trunk muscles
Forelimb-Hindlimb (FLHL) Whisker (WH)	Exclusive forepaw and HL ankle dorsiflexion movements Whisker movements	Coactivation of forelimb and hindlimb muscles Absence of any EMG response

Table 1. Movement type classification. Explanation of how movement types were determined for each intracortical microstimulation trial.

## Trunk motor cortex is somatotopically organized

To understand trunk musculature recruitment associated with the different coactivation zones, EMG responses were examined in more detail. As expected, stimulation of forelimb trunk cortex (FLT) preferentially activated spinous trapezius (SP) and contralateral upper thoracic longissimus (LUT). FLT coactivation zone is thus responsible for upper thoracic trunk muscles activation (Figure 5A-5C). Similarly, stimulation of hindlimb trunk cortex (HLT) activated the obliques along the mid and lower thoracic level and therefore HLT coactivation zone is preferentially responsible for mid and lower trunk muscles activation (Figure 5A-5C). Interestingly, stimulation of ET cortex also activated the oblique but at all thoracic levels, suggesting that ET is important to coordinate movements of the entire trunk. Finally, stimulation of the synergistic trunk cortex (FHT) activated mostly trunk musculature at the mid thoracic

level (Figure 5C). Therefore, the different trunk coactivation zones differentially activate segmental trunk muscles (upper, mid, and lower thoracic levels) providing topography to TrM1 motor control.

To gain more insight, we constructed two maps of trunk coactivation zone: the first to identify the proportion of penetrations across animals that activated upper trunk muscles (Figure 5D) and the second to identify the proportion that activated lower trunk muscles (Figure 5E). The mediocaudal region of trunk coactivation zone preferentially controlled lower thoracic trunk musculature while the rostrolateral region controlled upper thoracic trunk musculature. The lower trunk musculature was more influenced by the rostrolateral area of trunk coactivation zone and upper trunk musculature by the mediocaudal area of trunk coactivation zone. To demonstrate this topography along the rostrocaudal axis, the proportion of penetrations activating upper or lower thoracic trunk from mediolateral locations were averaged (Figure 5F). Moving rostral, there was an increase in the probability of activating upper trunk (Linear Regression,  $r^2 = 0.61$ , F [1, 11] = 17.82, p < 0.01), whereas moving caudal, there was an increase in the probability of activating lower trunk (Linear Regression,  $r^2 = 0.83$ , F [1, 11] = 54.70, p < 0.01). This demonstrates a clear somatotopy within the trunk coactivation zone that define subregions of TrM1: UTM1 and LTM1.

Considering that segmental trunk muscles were differentially activated within this trunk coactivation zone, the amount and extent of activation within the coactivation zone was examined using the responsiveness score. The responsiveness scores were similar across the mid, upper, and lower thoracic segmental levels (N = 54, each level) (One-way ANOVA, F [2, 159] = 0.49, p = 0.54; Figure 5G), suggesting that the probability of cortex to activate the different segmental levels exclusively is similar. However, despite this similarity, there were differences

in the likelihood of segmental coactivation (One-way ANOVA, F [3, 212] = 9.06, p < 0.001; Figure 5H) with the mid and lower thoracic muscles more likely to coactivate than other segmental muscle groups (Tukey's post-hoc test, p < 0.001). In summary, most of TrM1 is devoted to activation with other regions of the body and cortical representation of mid and lower thoracic trunk muscles are associated with hindlimb muscle representation while upper thoracic trunk muscles are associated with forelimb muscle representation. These results were confirmed by synergy analysis using the amplitude of evoked EMG responses obtained from the different trunk musculature (Supplementary Figure 1).

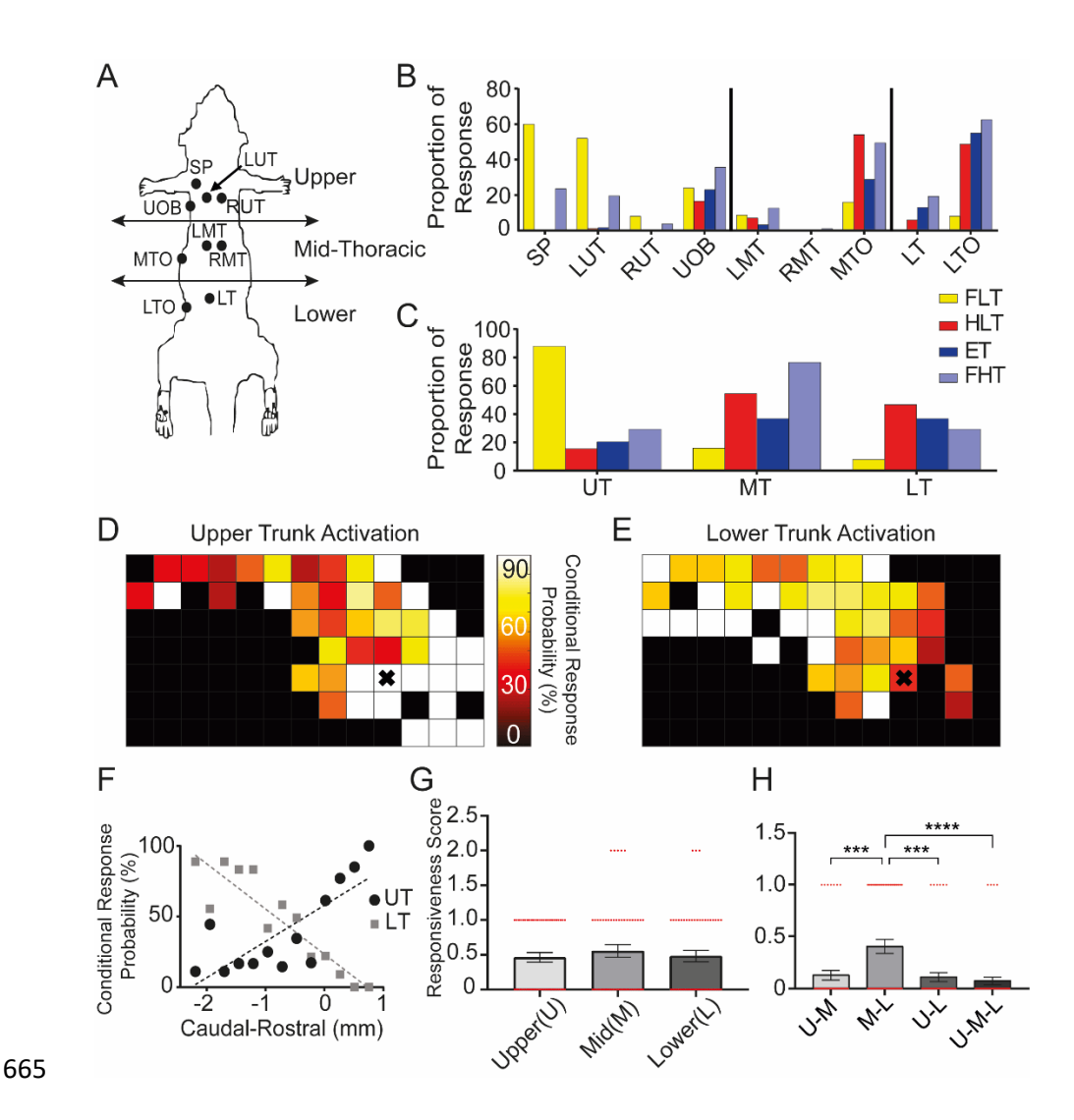


Figure 5. Recruitment of trunk musculature in the different coactivation zones. A) Methodological diagram showing EMG electrode locations of trunk muscles categorized into three groups along the rostrocaudal axis of the body: upper thoracic, mid thoracic, and lower thoracic trunk muscles. B) Proportion of muscle responses in the different coactivation zones by muscle. C) Same graph as B, but muscles are grouped within the three segmental zones seen in A. Upper thoracic muscles were activated when FLT coactivation zone was stimulated and lower thoracic muscles were activated when HLT coactivation zone was stimulated. D-E) For locations within TrM1, the conditional probability of activating upper trunk musculature (D) is compared to activating lower trunk musculature (E). The X location refers to 0 mm RC, 2 mm ML, relative to bregma. F) Graph showing the conditional probability of eliciting trunk muscle responses in TrM1 based on visual observation & EMG responses of either upper or lower trunk musculature averaged across the rostrocaudal axis G) Average responsiveness score within TrM1 (see Materials and Methods; N = 54) for the different segmental zones: upper, mid, and lower thoracic. H) Differences in the likelihood of segmental coactivation were also plotted within TrM1 for each of the segmental coactivations.

682		
	Trunk musculature type	EMG response
683	Dorsal Trunk	Activation of spinous trapezius or longissimus muscles at upper, mid, or lower thoracic level
684	Ventral Trunk	Activation of external oblique muscles at upper, mid, or lower thoracic level
685		,
686	Upper Thoracic Trunk (U)	Activation of spinous trapezius (SP), left upper thoracic longissimus (LUT), right upper thoracic longissimus (RUT), or upper external oblique (UOB)
687		
688	Mid Thoracic Trunk (M)	Activation of left mid thoracic longissimus (LMT), right mid thoracic longissimus (RMT), or mid thoracic external oblique (MTO)
689	Lower thoracic trunk (L)	Activation of lower thoracic oblique (LTO) or lower thoracic longissimus (LT)
690	Table 2 Tours and the second street in the	. Museles that were retired in account to interesting

Table 2. Trunk musculature classification. Muscles that were activated in response to intracortical microstimulation were classified as one of five muscle types.

700

701

702

703

704

705

706

707

708

709

710

711

712

713

714

715

716

717

718

719

720

Somatosensory input to trunk motor cortex is dominated by hindlimb information Given our understanding of somatosensory overlap within S1 and coactivation of trunk muscles with other regions of the body, we examined the integration of TrM1 with somatosensory input from the limbs by recording neural response in TrM1 supragranular and infragranular layers in response to electric stimulation of forelimbs, hindlimbs, mid trunk or upper trunk (Figure 6A). There was little to no response in TrM1 to low intensity stimulation (0.5 mA) applied to any of the four body locations. However, this was not the case for high intensity stimulation (5.0 mA). Surprisingly, the SEP amplitude recorded from TrM1 in response to high intensity somatosensory stimulation of the hindlimbs was greater than the SEP amplitude to stimulation of either mid or upper trunk (Figure 6B, 6C). The response to forelimb stimulation was similar to that of trunk stimulation, solidifying that TrM1 preferentially receives somatosensory information from hindlimbs. Due to the internal motor somatotopy along the rostrocaudal axis of TrM1 (refer to Figure 5F), cortical locations where SEPs were recorded were segregated into rostral (0 to -0.75 mm RC) and caudal regions (-1 to -2 mm RC). In the supragranular layer (Caudal, N = 103; Rostral N = 103) 96), there was no effect of recording location (Two-way ANOVA, F[1, 191] = 2.34, p = 0.13), but there was an effect of stimulus location (Two-way ANOVA, F [3, 191] = 22.25, p < 0.0001; Figure 6D) such that the SEP amplitude recorded from both rostral and caudal TrM1 in response to hindlimb stimulation was greater than the response to stimulation of all the other locations (Tukey's post-hoc test, p < 0.0001). This result demonstrates an important role for hindlimb somatosensory integration within TrM1, but without any somatotopic organization. Surprisingly, there was no difference in the SEP amplitude in response to upper trunk stimulation compared to

721 mid trunk stimulation (Tukey's post-hoc test, p = 0.99), suggesting no somatotopy of trunk somatosensory input within TrM1. 722 723 In the infragranular layer (Caudal N = 95; Rostral N = 85), there was again an overall effect of 724 stimulus location (Two-way ANOVA, F [3,172] = 14.48, p < 0.0001; Figure 6E), where the SEP amplitude to hindlimb stimulation was again greater in both the caudal and rostral region of 725 726 TrM1 suggesting that hindlimb somatosensory input to TrM1 was evenly distributed, across 727 supra- and infragranular layers, between LTM1 and UTM1 as suggested by Figure 6C. 728 Moreover, like the supragranular layer, there were no differences between SEP amplitude in 729 response to mid trunk stimulation compared to upper trunk stimulation (Tukey's post-hoc test, p = 0.95), suggesting similar organization for both supra and infragranular layers. Finally, to assess 730 731 the effectiveness of high intensity (5.0 mA) hindlimb stimulation to reach the sensory or motor cortices, the SEP amplitude was compared across  $\frac{\text{TrM1}}{(N=8)}$ ,  $\frac{\text{TrS1}}{(N=5)}$ ,  $\frac{\text{HLS1}}{(N=7)}$ . 732 and FLS1 (N = 5). There was an overall effect of cortical location (One-way ANOVA, F [3, 21] 733 = 10.14, p < 0.001; Figure 6F), and as expected, the SEP response in HLS1 was greater than the 734 response in any other region (Tukey's post-hoc test, HLS1 vs TrS1, p < 0.001; HLS1 vs TrM1, p735 < 0.01; HLS1 vs FLS1, p < 0.001). These results further support the extensive and preferential 736 737 integration of hindlimb somatosensory input into TrM1.

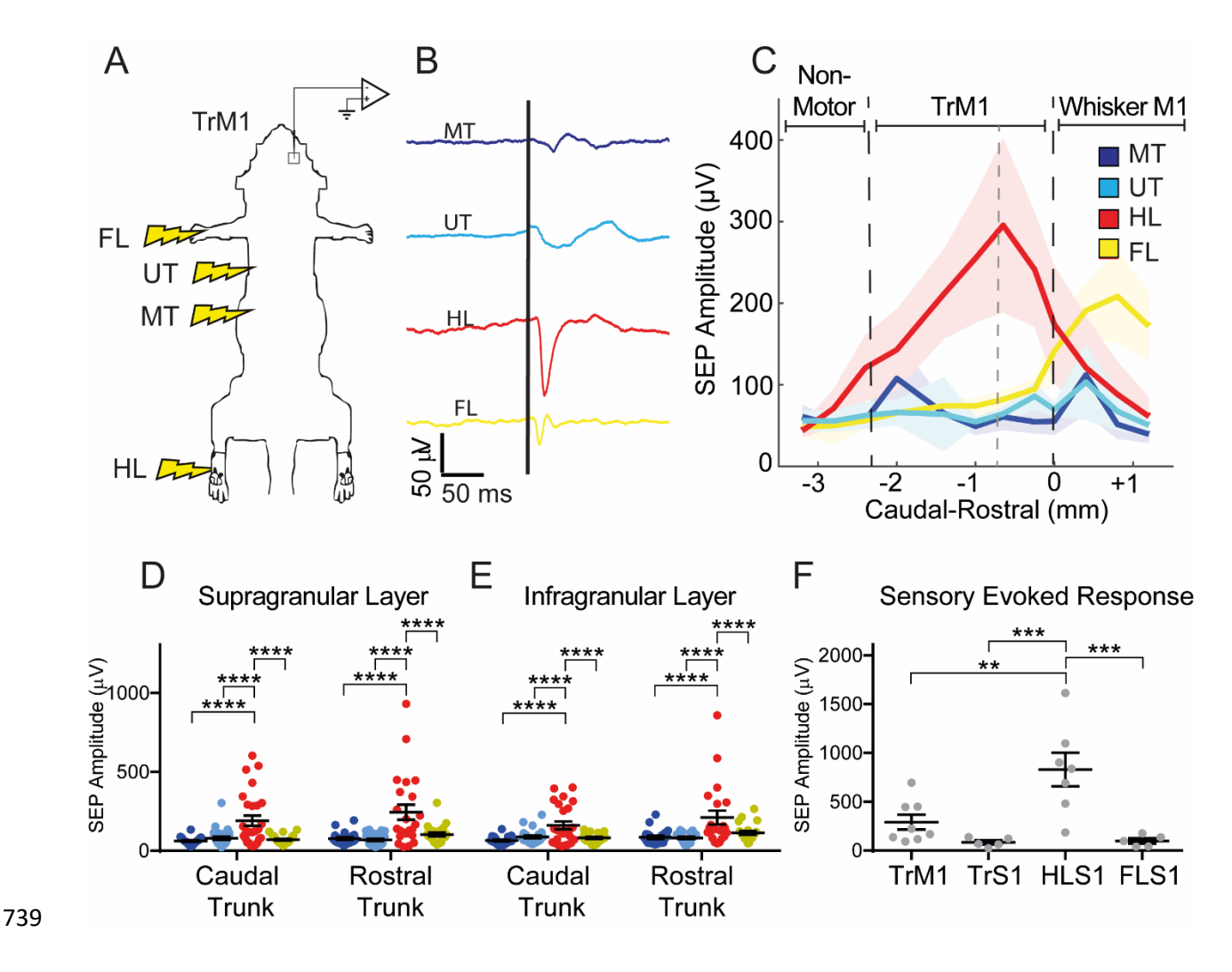


Figure 6. Response to high intensity hindlimb stimulation predominates in trunk M1. A) Methodological diagram of the 5.0 mA electrical stimulation paradigm. Stimulations occurred in the dorsal hairy skin of forelimb (FL), hindlimb (HL), T4-T5 dermatome (UT), and T9-T10 dermatome (MT). B) Example of somatosensory evoked responses in TrM1 from the different stimulation locations on the body. C) SEP amplitude in the supragranular layer in response to stimulation across the rostrocaudal axis of TrM1 at 1.25 mm ML. Dotted line within TrM1 represents the distinction between caudal and rostral trunk. D-E) SEP amplitude in the supragranular (Caudal, N = 103; Rostral N = 96) (D) and infragranular (Caudal N = 95; Rostral N = 85) (E) layers in the caudal region (-1 mm to -2 mm RC, relative to bregma) and in the rostral region (-0.75 mm to 0 mm RC, relative to bregma) of the TrM1. Rostral regions activate upper thoracic musculature, while caudal regions activate lower thoracic trunk musculature. F) Somatosensory evoked response in the supragranular layer of TrM1 (N = 8), TrS1 (N = 5), HLS1 (N = 7), and FLS1 (N = 5) from hindlimb stimulation.

### Sensorimotor integration is cortico-cortical for trunk stimuli, thalamo-cortical for

#### hindlimb stimuli

Since sensorimotor integration in the cortex can be mediated by projections from the S1 cortex and the thalamus (Canedo 1997; Mao et al. 2011; Hooks 2016), retrograde tracing was used to better understand the relative contribution of cortico-cortical versus thalamo-cortical connections

to TrM1 (Figure 7A). Tracer injected into the location most likely to contain the exclusively trunk region revealed that TrM1 received cortico-cortical input from ipsilateral TrS1, HLS1, and FLS1. As expected, given the variability across animals in the location of exclusively trunk cortex, the relative contribution from these sensory cortices was variable across animals (Figure 7B). Rats 1 and 2 had more cells projecting to TrM1 from HLS1 than from TrS1, while rat 3 showed projections exclusively from dorsal TrS1, and rats 4 and 5 showed projections predominately from dorsal TrS1. TrM1 also received input from secondary sensory cortex, dysgranular zone, whisker, and face S1 (data not shown), thereby making TrM1 a crossroad for somatosensory information. In all animals, the projections from S1 to TrM1 were predominantly mediated by S1 cells in the supragranular and infragranular layers (Figure 7C). This laminar specificity is consistent with studies in the whisker sensorimotor system (Mao et al. 2011; Hooks et al. 2013). Tracing also revealed strong thalamo-cortical projections from the ventral posterolateral nucleus (VPL) of the thalamus to TrM1 in all animals (Figure 7D, 7E) that likely carries proprioceptive information (Francis et al. 2008), however, tactile information from the thalamus cannot be ruled out. To determine if the source of projections to TrM1 differed between body parts that were stimulated, SEP latency was analyzed. The mean latency of the SEP recorded from TrM1 (26.84 +/- 2.65 ms) was significantly longer than that from TrS1 (20.30 +/- 0.83 ms) when mid trunk was stimulated (Independent Samples t-test, t [12] = 2.66, p < 0.05; Figure 7F). This led us to conclude that the sensorimotor integration of trunk somatosensory information in TrM1 is primarily mediated by cortico-cortical projections. In contrast, the mean latency of the SEP recorded from TrM1 (23.44 +/- 1.81 ms) was similar to the that from HLS1 (21.15 +/- 1.66 ms) when hindlimb was stimulated (Independent Samples t-test, t [12] = 0.90, p = 0.39; Figure 7F

755

756

757

758

759

760

761

762

763

764

765

766

767

768

769

770

771

772

773

774

775

776

and see Supplemental Figure 3). This led us to conclude that the integration of hindlimb somatosensory input in TrM1 is primarily mediated by thalamo-cortical projections, carrying somatosensory information, including proprioceptive. To identify how this somatosensory information might be used, next we recorded single neurons from TrS1 and TrM1 while animals were subjected to tilts in the lateral plane.

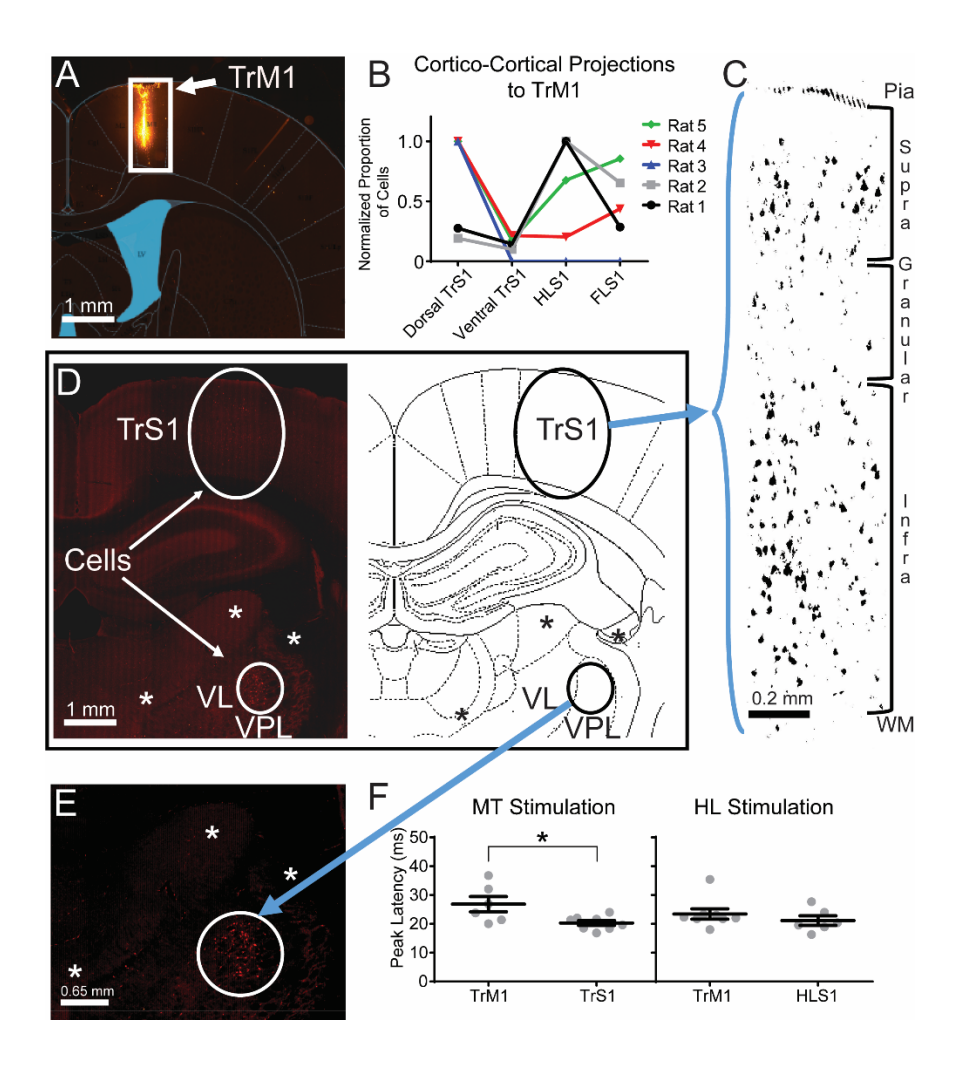


Figure 7. Cortico-cortical and thalamo-cortical projections to trunk M1. A) Coronal brain slice with a superimposed rat brain atlas image (Paxinos and Watson 2007). The injection site (-0.5 mm RC, 1.25 mm ML, 1.65 mm DV, relative to bregma) was limited to TrM1. Scale bar: 1 mm. B) Proportion of cells, normalized to the maximum number of cells across all cortical regions sampled within an animal, in the different primary sensory cortices (dorsal trunk S1, ventral trunk S1, hindlimb S1 and forelimb S1; for coordinates see Materials and Methods). Most TrM1 projecting cells are located in TrS1 and HLS1. (Rat number: raw number of cells in dorsal TrS1, ventral TrS1, HLS1, and FLS1; Rat 1: 229, 120, 830, 237; Rat 2: 62, 32, 323, 211; Rat 3: 257, 0, 0, 0; Rat 4: 1886, 404, 384, 826; Rat 5: 1344, 236, 908, 1149.) C) Black and white image of the labelled cortical cells in a coronal view of TrS1. Most of the neurons are located in the supra and infragranular layers. Scale bar: 0.2 mm. D) Image of the labelled cortical and thalamic cells in a coronal view with the corresponding modified rat brain atlas. Thalamic neurons are located in the VPL of the thalamus as the thalamic nuclei borders can be seen in both the left image and in the right atlas. The "\*" indicates

corresponding structures to help the viewer localizing the different thalamic nuclei. Scale bar: 1 mm. E) Zoomed in image of D to visualize the labeled cells in the VPL of the thalamus. The contrast has been increased in order to specifically focus on the presence of the labeled cells. The "\*" indicates the same locations as in D to aid the viewer in locating the cells. Scale bar: 0.65 mm. F) Left: peak latency of the high intensity mid trunk stimulation in  $\frac{1}{1}$  TrM1 (N = 6) and  $\frac{1}{1}$  Right: peak latency of the high intensity hindlimb stimulation in  $\frac{1}{1}$  TrM1 (N = 8) and HLS1 (N = 6).

## Postural control is predominately supported by hindlimb somatosensory and lower trunk

#### motor cortices

794

795

796

797

798

799

800

801

802

803

804

805

806

807

808

809

810

811

812

813

814

815

816

817

818

819

To investigate the importance of sensorimotor integration between trunk and hindlimb in postural control, animals were subjected to unexpected tilts in the lateral plane during a tilt task (Bridges et al. 2018), while single units were recorded from the following S1 and M1 cortices: FLS1 (n = 68), HLS1 (n = 39), TrS1 (n = 237), HLM1 (n = 124), and TrM1 (n = 325); Figure 8A, 8B). Three measures from the neuronal data were compared: responsiveness (i.e., proportion of neurons responding), magnitude of the single neuron response, and mutual information carried by the response regarding the severity of the tilt (Figure 8C-8H). First, the proportion of responsive cells was compared between S1 regions (FLS1: 57%, TrS1: 32%, HLS1: 82%). TrS1 was less responsive than HLS1 ( $\chi^2$  [1, N = 276] = 35.84, p < 0.0001) or FLS1 ( $\chi^2$  [1, N = 305] = 14.92, p < 0.001), and HLS1 cells were more likely to respond than FLS1 ( $\chi^2$  [1, N = 107] = 6.77, p < 0.01; Figure 8C). Moreover, the magnitude of the TrS1 response (1.87+/- 0.19 spikes per second) was smaller than that of HLS1 (3.32 +/- 0.36 spikes per second) or FLS1 cells (2.94 +/- 0.32 spikes per second) during the tilt task (One-way ANOVA, F [2, 145] = 8.63, p < 0.001, Tukey's post-hoc test: HLS1 vs TrS1 [p < 0.001], FLS1 vs TrS1 [p < 0.05]; Figure 8D). Lastly, mutual information was compared between S1 regions. The median mutual information carried by TrS1 (0.04, [0.03] bits) was significantly less than the median mutual information carried by FLS1 (0.05 [0.06] bits) or HLS1 (0.06 [0.07] bits) during the tilt task (Kruskal-Wallis test, H [2] = 21.73, p < 0.0001, Dunn's post-hoc test: HLS1 vs TrS1 [p < 0.001], FLS1 vs TrS1 [p < 0.01]; Figure 8E). Thus, TrS1 conveyed less mutual information and was less discriminative of the type

of tilt than FLS1 or HLS1. Importantly, after dividing TrS1 into LT, MT, and UT (see Materials 820 and Methods), there were no differences between these trunk subregions in responsiveness 821 (LTS1: 50%, MTS1: 38%, UTS1: 28%;  $\chi^2$  [2, N = 237] = 5.64, p = 0.06). The magnitude of 822 response significantly differed between these TrS1 subregions (LTS1: 2.25 [1.93], MTS1: 0.88 823 [1.23], UTS1: 1.59 [1.59]; Kruskal-Wallis test, H[3] = 6.67, p < 0.05); however, Dunn's post-824 825 hoc test did not reveal any significant pairwise comparisons. Additionally, there were no differences in mutual information between subregions (LTS1: 0.04 +/- 0.004, MTS1: 0.06 +/-826 0.01, UTS1: 0.06 +/- 0.01; One-way ANOVA, F[2, 234] = 0.43, p = 0.65; Figure 8C-8E), 827 suggesting that the entire TrS1 is equally engaged in this task. 828 On the other hand, TrM1 neurons were equally likely to respond to the task compared to HLM1 829 neurons (HLM1: 63%, TrM1: 72%; Fisher's exact test, N = 449, p = 0.07; Figure 8F), though 830 neither the magnitude of the response (HLM1: 3.42 +/- 0.30 spikes per second, TrM1: 4.05 +/-831 0.23 spikes per second; Independent Samples t-test, t [311] = 1.46, p = 0.14; Figure 8G), nor 832 their mutual information (HLM1: 0.07 [0.08] bits, TrM1: 0.06 [0.08]; Mann-Whitney test, U =833 19112, p = 0.40; Figure 8H) differed from HLM1. Interestingly, when examining the responses 834 from different subregions within TrM1, LTM1 was more involved than UTM1. In fact, even 835 836 though neurons in LTM1 had a similar proportion of cells responding to the tilts compared to UTM1 (LTM1: 76%, UTM1: 69%;  $\chi^2$  [1, N = 325] = 2.32, p = 0.12; Figure 8F), the magnitude of 837 the response of LTM1 neurons was greater than that of UTM1 neurons (LTM1: 4.57 +/- 0.35, 838 UTM1: 3.46 +/- 0.27; Independent Samples t-test, t [233] = 2.49, p < 0.05; Figure 8G). This 839 resulted in more information about the severity of the tilt being encoded by LTM1 compared to 840 UTM1 (LTM1:0.07 [0.09] bits, UTM1: 0.06 [0.06] bits; Mann-Whitney test, U = 11063, p < 100841 0.05; Figure 8H). These data suggest that LTM1 may be specialized for postural control. 842

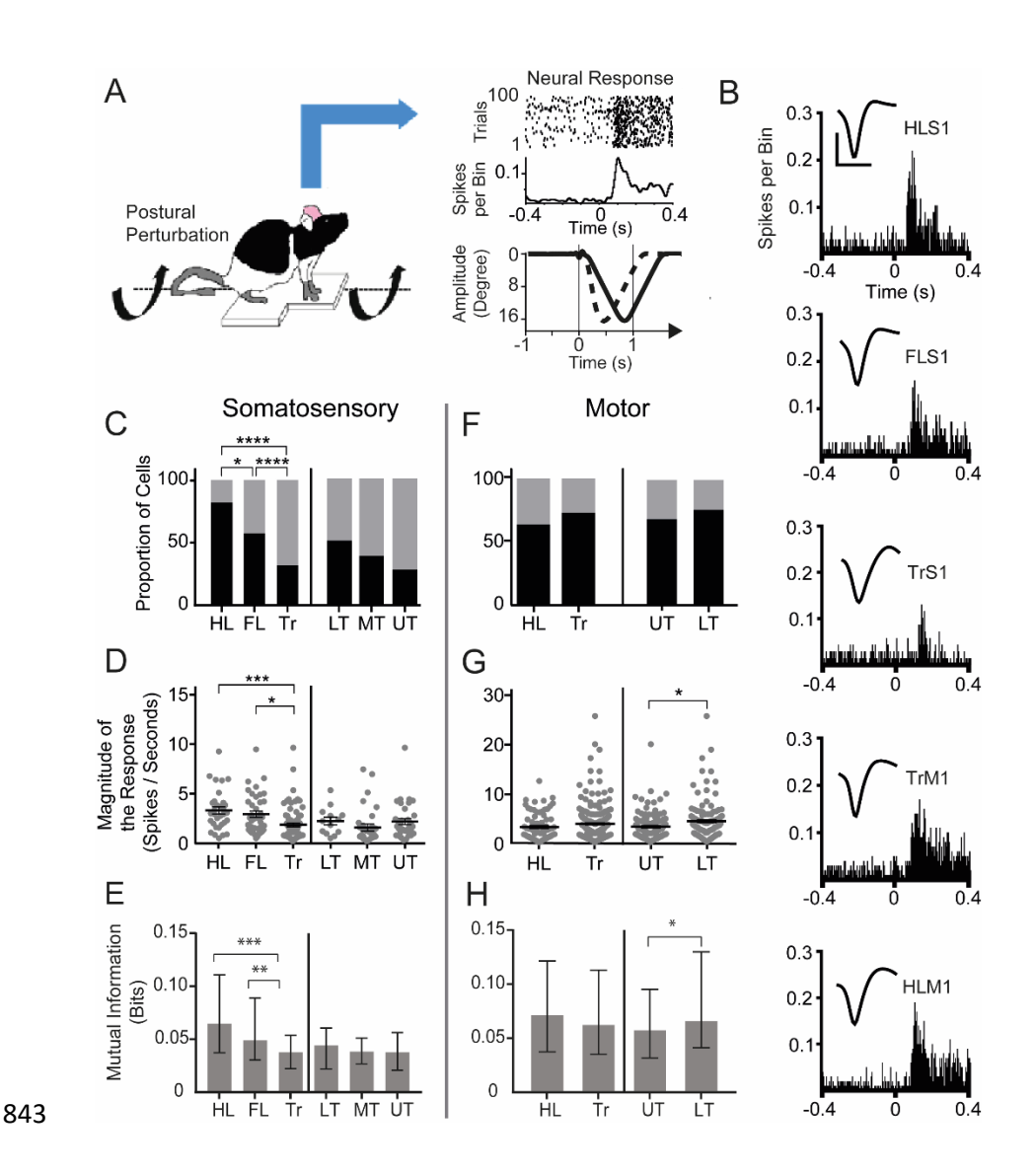


Figure 8. Hindlimb S1 and lower trunk M1 combine to carry the most information about postural control. A) Methodological diagram of the postural control task. The animal experienced unexpected tilts in the lateral plane while single neurons in different sensory and motor cortices were recorded (upper right panel). The bottom right panel shows the tilt profile for the fast (dotted line) and the slow (unbroken line) tilt events, applicable for both directions (left and right). B) Example PSTHs showing a neuron response to the unexpected tilt for each recorded cortical area in the sensory and motor cortices. The waveform scale on top: y-axis: 0.05 mV, x-axis: 0.6 ms. C) Responsiveness of different sensory cortices. Data presented as cortical area: (number of responsive cells, number of non-responsive cells, % of responsive cells). HLS1: (32, 7, 82%), FLS1: (39, 29, 57%), TrS1: (80, 157, 34%), LT: (13, 13, 50%), MT: (31, 51, 38%), UT: (36, 93, 28%). D) Magnitude of the response (for responsive cells only) in different sensory cortices. E) Mutual information in different sensory cortices (represented as median +/- interquartile range for all cells [responsive cells, number of non-responsive cells, % of responsive cells). HLM1 (78, 46, 63%), TrM1 (235, 90, 72%), LTM1 (111, 51, 76%), UTM1 (124, 39, 69%). G) Magnitude of the response (for responsive cells only) in different motor cortices. H) Mutual information in different motor cortices (represented as median+/- inter quartile range for all cells [responsive and non-responsive)].

860 Discussion

861

862

863

864

865

866

867

868

869

870

871

872

873

874

875

876

877

878

879

880

881

882

Together, these data present an extensive view describing how cortical organization is relevant to function by demonstrating the preferential interplay between trunk and hindlimb (Figure 9). Summarizing, TrS1 and TrM1 are larger than previously reported and there is relevant somatotopy within both. In addition, TrS1 receives input from other body regions, especially the hindlimbs, and TrM1 largely coactivates trunk muscles with muscles from other body regions, especially the hindlimbs. Regarding sensorimotor integration, somatosensory information from the hindlimbs is more likely to be integrated within TrM1 than that from forelimbs or even trunk. The functional role of this integration of hindlimb somatosensory information within TrM1 for postural control was demonstrated by the relative difference in the mutual information carried by hindlimb and trunk sensory and motor cortices to tilts in the lateral plane recorded from awake animals. On the sensory side, HLS1 and FLS1 are more involved than TrS1 during postural perturbations. While on the motor side, HLM1 and TrM1 are equally involved, with LTM1 more involved than UTM1. This has important implications for recovery of function after neurological injury or disease (Knudsen and Moxon 2017; Manohar et al. 2017; Bridges et al. 2018) and is discussed below.

#### **Methodological considerations**

Choices made in our experimental design impacted data analysis. First, for sensory maps, we chose to record from as many single units as possible, identifying the extent of each cell's receptive field as our recording electrode was passed through the entire depth of S1. Therefore, it was not possible to sample the entire TrS1 within a single animal due to time constraints.

Similarly, for TrM1, we chose to sample from as many muscles as possible, adding to the length of the surgery and limiting our ability to sample the entire TrM1 within every animal. Moreover,

here we show that, unlike the whisker, forelimb, and hindlimb sensory systems that tend to have differences in RF size across layers (Chapin 1986), the RF size of neurons in TrS1 was similar across layers, within the same RF center. However, the role of urethane anesthesia in this assessment cannot be ruled out (Friedberg et al. 1999). Furthermore, within S1, the responses to both low and high intensity stimuli are likely to be a combination of tactile and proprioceptive information, with the low intensity stimulation predominately eliciting tactile information and the high intensity stimulation adding additional proprioceptive information. In comparison to S1, low intensity stimuli did not elicit responses within M1; however, high intensity stimuli induced muscle twitches. Thus, in M1, a greater proportion of responses to high intensity stimuli were likely proprioceptive than tactile. The tracing study suggests that somatosensory information, a mix of tactile and proprioceptive information, reaches TrM1 from S1 and thalamus. The latency studies suggest that the predominate response in TrM1 to mid trunk stimulation arrives from the somatosensory cortex. Alternatively, the predominate response in TrM1 that is elicited by hindlimb stimulation likely arrives from the VPL of the thalamus. The VPL origin of this response, which predominately carries proprioceptive information, further supports that the response in TrM1 to high intensity stimulation of the hindlimbs carries more proprioceptive information than the low intensity stimulation, although more work would need to be done to confirm this.

883

884

885

886

887

888

889

890

891

892

893

894

895

896

897

898

899

900

901

902

903

904

905

#### Oppositional gradient in overlap across thoracic dermatomes from DRG to trunk S1

Overlap of somatosensory information from the trunk varies along the entire neural axis. At the spinal level, overlap between thoracic dermatomes is graded such that caudal DRGs (T10-T13) have less overlap than rostral DRGs (T1-T5). At the same time, representation of these dermatomes in S1 have the opposite gradient regarding overlap. The RF size of TrS1 neurons

increased along the mediolateral axis of cortex, such that the lower thoracic TrS1 neurons had a greater RF size compared to the upper thoracic TrS1 neurons. This change in RF size across TrS1 has also been shown in the ventral trunk representation (Xerri et al. 1994). Taken together, for a given stimulation to lower trunk dermatomes, the limited overlap results in fewer DRGs conveying somatosensory information to the cortex where S1 neurons with larger receptive fields amplify the signal. In contrast, for upper trunk dermatomes, the greater overlap across DRGs amplifies information to the cortex where neurons have smaller receptive fields. Therefore, the lack of overlap at the spinal level is compensated for by the greater overlap at the cortical layer and vice versa. The functional implication of this is that dorsal rhizotomy of a caudal DRG would result in a more complete deafferentation than a dorsal rhizotomy of a rostral DRG. It may be that due to the dexterous use of the forelimbs, it is considered more important to preserve upper trunk than lower trunk somatosensory information.

#### Trunk sensorimotor integration supports a range of functions

The present data suggest that trunk muscles serve as a biomechanical link between the forelimbs and hindlimbs even in the absences of a neonatal spinal cord transection (Giszter et al. 2010). Moreover, this linkage combines somatosensory information across the limbs and trunk, especially the hindlimbs. In the intact adult, our data show extensive overlap of trunk somatosensory signals within FLS1 and HLS1, especially in response to high intensity stimuli, thereby suggesting that HLS1 is modulated by the location and movement of trunk in space, which could be used to guide the lower limbs during locomotion (Rossignol et al. 2006). At the same time, somatosensory information from hindlimb and forelimb overlap within TrS1, which confirms the importance of integrating information from the limbs with trunk somatosensory processing. Within M1, trunk muscles are more likely to coactivate with hindlimb than trunk

muscles or forelimb muscles alone. Furthermore, approximately half of the animals had coactivation of forelimb and hindlimb muscles without concomitant activation of trunk muscles (data not shown). The area was located within the synergistic trunk region. This coactivation of forelimb and hindlimb was also found in other species across phylogenic scales, such as the mouse (Li and Waters 1991), tree squirrel (Cooke et al. 2012), tree shrew (Baldwin et al. 2017), prosimian Galagos (Stepniewska et al. 2005), and macaque monkey (Baldwin et al. 2018). These synchronous forelimb-hindlimb coactivations (Halley et al. 2020) are thought to be involved in a range of movement types associated with locomotion (e.g., galloping; Lemieux et al. 2016). The work presented here extends this understanding by highlighting the greater integration between trunk and hindlimb than trunk and forelimb. Classical studies showed that sensory information in M1 was mainly homotopic. For example, neurons in whisker M1, FLM1, and HLM1 received somatosensory input from the same body part that induced movement when activated with ICMS (Asanuma et al. 1968; Rosén and Asanuma 1972). However, our data suggest that the TrM1 is unique in that it receives somatosensory information from trunk, hindlimbs and forelimbs, and therefore the integration of sensorimotor information within TrM1 is not strictly homotopic. Indeed, while low amplitude somatosensory stimulation of trunk, hindlimb or forelimb did not impact TrM1, high amplitude stimulation of HL produced a greater response in TrM1 than somatosensory stimulation of either trunk or forelimb. As many studies have demonstrated that somatosensory feedback to the motor cortex is critical during locomotion and recovery of function after spinal cord injury (Hicks and D'Amato 1975; Rossignol et al. 2006; Beaumont et al. 2014; Moreno-López et al. 2016; Knudsen and Moxon 2017; Manohar et al. 2017), understanding how the post-injury

929

930

931

932

933

934

935

936

937

938

939

940

941

942

943

944

945

946

947

948

949

sensorimotor integration differs from the integration shown here will be important for interpreting these injury studies.

Combined, this extensive sensory overlap, muscle coactivations, and heterotopic sensory integration between the trunk and the limbs supports communication between trunk sensory and motor cortices within the broader sensorimotor cortex to achieve optimal behavior. For example, it has been previously shown that the lower thoracic trunk muscles play an important role in sexual posturing and lordosis as observed in the female rat (Brink and Pfaff 1980). Our results show that the caudal portion of TrM1 that controls these lower thoracic muscles overlaps with the genital motor cortex (Lenschow and Brecht 2018). The extensive integration of hindlimb somatosensory information within TrM1 could be useful for sexual posturing.

#### Role of trunk sensorimotor cortex in postural control

The integration of HL somatosensory input across the extent of TrM1combined with the broad hindlimb-trunk coactivation zones in M1 support the role of thoracic trunk muscles synergistically acting with the hindlimbs to aid in postural control during locomotion (Anders et al. 2007; Song et al. 2015; Bridges et al. 2018). This coactivation likely happens through the cortico-reticulo-spinal pathway, not directly via the corticospinal pathway. In the awake animal, the vestibular system, which was not studied here, produces a fast reaction to control posture and recover balance (Murray et al. 2018). Notably, it sends direct motor inputs to the spinal cord to correct the balance. This vestibular information also ascends through the thalamus to the motor cortex to produce a coordinated neuronal response across the body musculature during the tilt (Horak and Jacobs 2007; Whelan 2009). Interestingly, the motor cortex participates in some, but not all, aspects of postural control (Deliagina et al. 2007; Horak and Jacobs 2007), producing different responses depending on the task despite similar muscle output (Karayannidou et al.

2009). Given the critical role of M1 for functional improvement after SCI (Manohar et al. 2017), improving our understanding of how information about postural adjustments is integrated in M1 will aid in understanding how M1 contributes to recovery of function (see next section). For example, in S1, previous studies showed that tactile and proprioceptive somatosensory feedback from the limbs are involved in postural control (Deliagina and Beloozerova 2000; Beloozerova et al. 2003). This is consistent with our data here showing that for both HLS1 and FLS1, more cells respond, and the magnitude of their response was greater compared to that of TrS1, such that FLS1 and HLS1 convey more information about the tilt than TrS1. But, within TrS1, the different areas of trunk (LT, MT, and UT) are equally responsive, conveying similar amounts of information about tilt. We can deduce that the response in TrS1 is predominately mediated by trunk proprioceptive information because the trunk is not in contact with the platform. Furthermore, because this study showed that a significant proportion of neurons in TrS1 responded to HL somatosensory information during the tilt task, the somatosensory information reaching TrS1 comes from the position of both the trunk and hindlimb in space, allowing significant integration of this proprioceptive information, along with tactile and vestibular, to allow the animal to maintain its balance. In the motor cortex, a similar proportion of HLM1 and TrM1 cells were likely to respond with a similar magnitude of response, conveying a similar amount of information about the tilt, suggesting that these two regions are equally active in controlling muscles when the animal is maintaining its balance in response to the tilt. Interestingly, within TrM1, the region that controls lower thoracic muscles (LTM1) was more engaged in the task compared to the regions that control upper thoracic musculature (UTM1). Given that more of the weight of the animal is over

974

975

976

977

978

979

980

981

982

983

984

985

986

987

988

989

990

991

992

993

994

the hindlimbs, these data suggest that extensive coactivation across hindlimb and lower thoracic muscles is used for postural control.

# Hindlimb somatosensory feedback to the trunk motor cortex: Pathophysiological

Pathologies resulting in postural deficits in humans are associated with changes in cortical

996

997

998

999

1000

1001

1002

1003

1004

1005

1006

1007

1008

1009

1010

1011

1012

1013

1014

1015

1016

1017

1018

**implications** 

organization (Tsao et al. 2008), motor planning (Hodges 2001), and recruitment of trunk musculature (Tsao et al. 2011). The integration of hindlimb proprioceptive information in TrM1 cortex identified here provides an opportunity for a new understanding of how therapy after mid thoracic spinal cord injury improves function. For a complete spinal transection, we previously showed that therapy produced sprouting of descending corticospinal axons from HLM1 cortex into thoracic spinal cord that could be used to control trunk musculature. This produced a larger representation of the TrM1 cortex whose extent was correlated to recovery of function and overlapped with expansion of the FLS1, creating a new circuit of forelimb somatosensory and trunk motor integration (Ganzer et al. 2016). If this reorganized cortex was lesioned, functional gains were lost (Manohar et al. 2017). Our new understanding of the extensive sensorimotor integration in intact animals presented here makes it more clear that the sensorimotor integration in animals that receive therapy after SCI is not a novel sensorimotor integration, but a necessary restoration of a system that operates on strong sensorimotor organization. While the role of limb proprioception after more severe injuries is less understood, our group previously showed that after complete spinal transection, when somatosensory input from the hindlimb is not possible, epidural stimulation induces somatosensory feedback from the trunk

into the deafferented hindlimb sensorimotor cortex that carries information about the animal's

behavior (Knudsen and Moxon 2017). This study now makes clear that this somatosensory

feedback is likely to be trunk proprioceptive information that provides input to hindlimb S1 and M1 cortices in intact animals. Therefore, therapy to improve function could take advantage of this pre-existing sensorimotor integration to restore function. This role of sensorimotor integration extends to models of partial spinal lesion. Proprioceptive information has been suggested to be critical for recovery of function after mid thoracic spinal cord injury (Edgerton et al. 2008). For example, epidural stimulation of spinal circuitry below the level of the lesion restored volitional locomotion in rats (Van Den Brand et al. 2012; Knudsen and Moxon 2017; Asboth et al. 2018), non-human primates (Capogrosso et al. 2016), and humans (Harkema et al. 2011; Rejc et al. 2017; Formento et al. 2018). Stimulation is conducted at lateral sites, over or near the DRGs and it has been suggested that this epidural stimulation activates proprioceptive afferents (Takeoka et al. 2014; Formento et al. 2018). Therefore, the work outlined in this paper supports the idea that facilitation of sensorimotor integration across broad regions of the cortex is key to improving treatment outcomes after neurological damage or disease (Ingemanson et al. 2019) and we now understand that this sensorimotor integration is the operational model of the trunk cortex in intact animals. Moving forward, our understanding of the sensorimotor integration in the intact system could be used to tailor rehabilitative strategies to optimize sensorimotor integration or recovery of function.

1019

1020

1021

1022

1023

1024

1025

1026

1027

1028

1029

1030

1031

1032

1033

1034

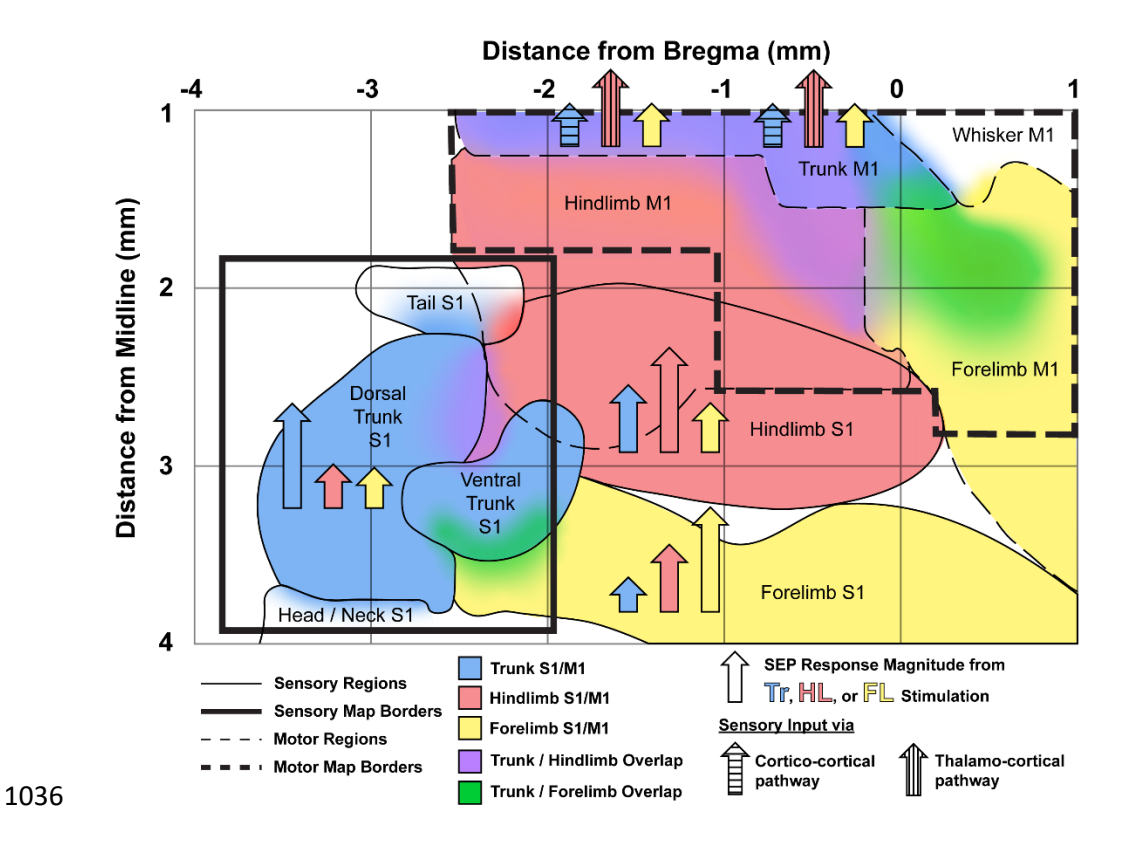
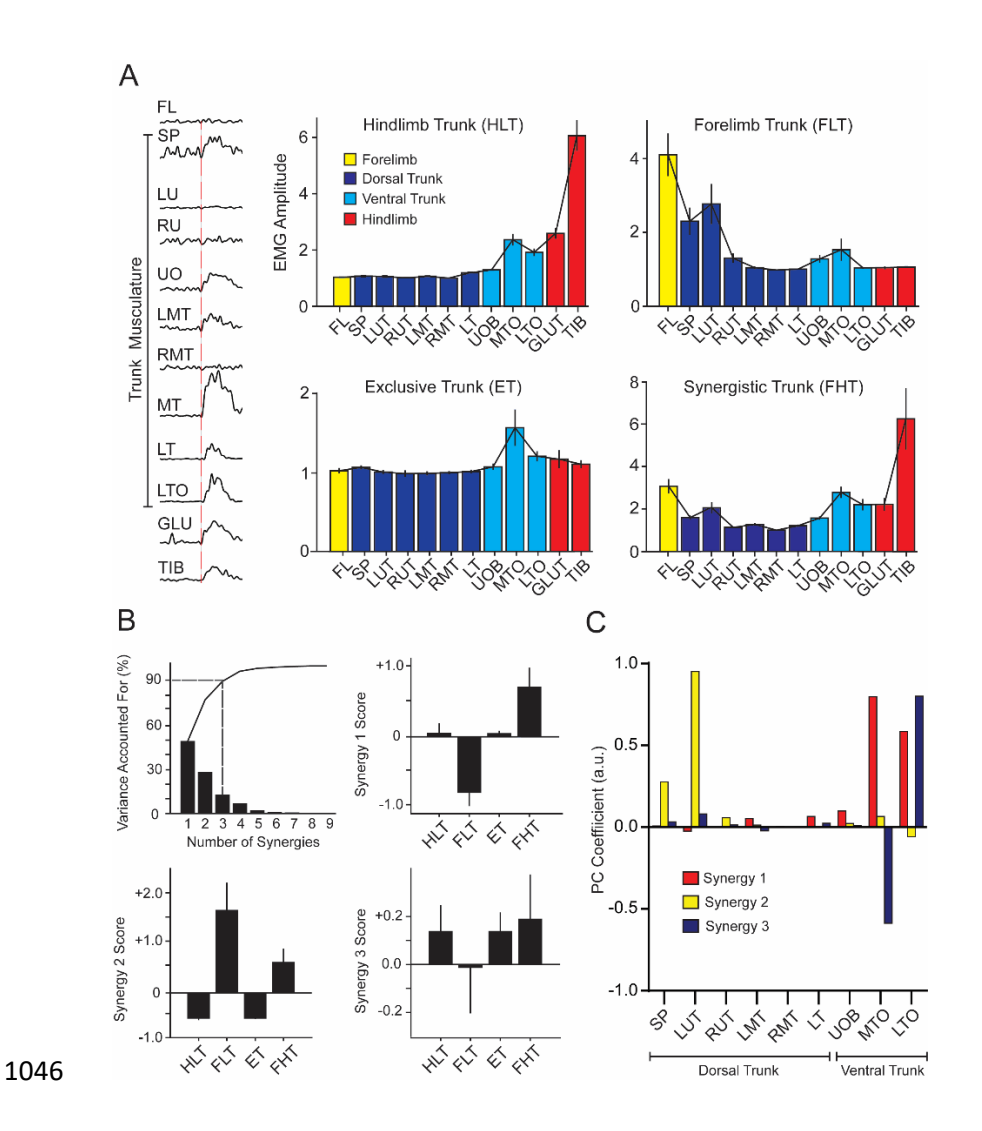


Figure 9. Summary of somatosensory overlap, motor coactivations and sensorimotor integration. Solid border lines indicate sensory regions while dashed border lines indicate motor regions. Bolded lines indicate the areas of S1 and M1 that were mapped in the current study. All other regions outside of these areas were adapted from (Xerri et al. 1994) and (Leergaard et al. 2004). Corresponding S1/M1 regions (e.g., trunk S1 / trunk M1) are represented with the same colors, while overlapping S1 regions or coactivating M1 regions are represented by the combined colors of the neighboring regions. Arrow height represents the relative magnitude of SEP responses within each cortical region from 5.0 mA stimulation of the trunk (blue), hindlimb (red), and forelimb (yellow). Horizontal (cortico-cortical) and vertical (thalamo-cortical) stripe patterns within each stimulation type's arrow indicates the predominate pathway for that type of sensory information to reach TrM1.



1048

1049

1050

1051

1052

1053

1054

1055

1056

1057

1058

1059

1060

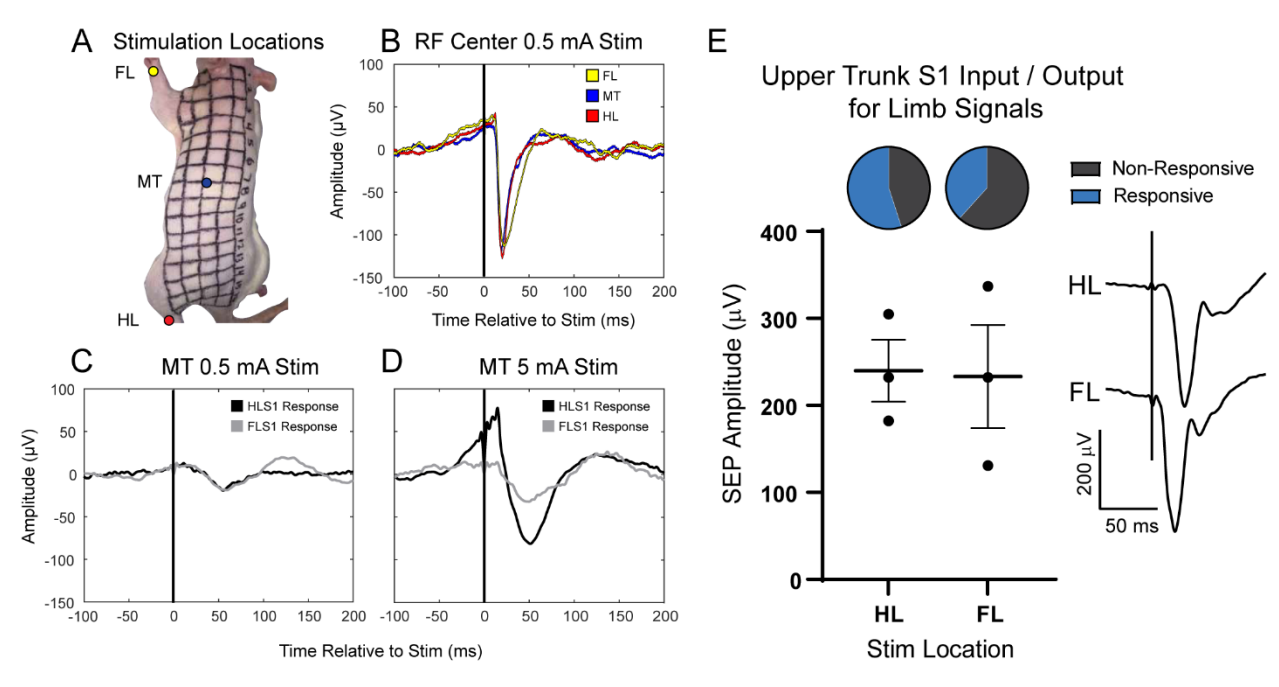
1061

1062

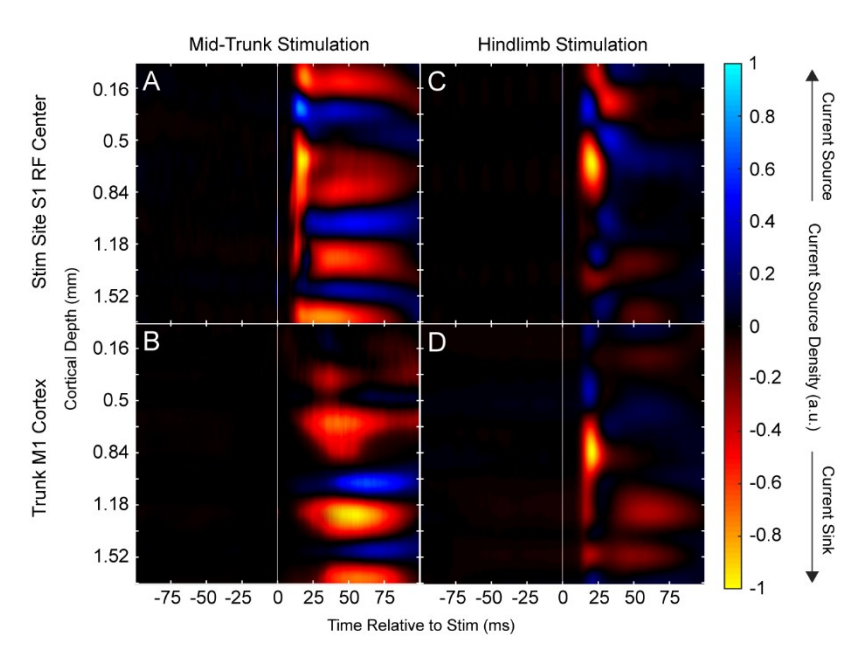
1063

1064

Supplemental Figure 1. Muscle synergy analysis of the different coactivation zones in trunk M1. A) Average MEP amplitude within the different coactivation zones (HLT [N = 174], FLT [N = 38], FHT [N = 85], and ET [N = 10]). EMG electrodes implanted along the trunk, forelimb, and hindlimb musculature (Top to bottom: Forelimb bicep [bicep], spinous trapezius [SP], left upper thoracic longissimus [LUT], right upper thoracic longissimus [RUT], upper external oblique [UOB], left mid thoracic longissimus [LMT], right mid thoracic longissimus [RMT], mid thoracic external oblique [MTO], lower thoracic longissimus [LT], lower thoracic external oblique [LTO], gluteus maximus [Glut], tibialis anterior [Tib]). B) PCA was performed to identify muscle synergies and their synergy scores were plotted. C) Synergy weights: Relative contribution of every trunk muscle towards the synergy was plotted. Three synergies were extracted that accounted for 90% of the cumulative variance in the data. Synergy 1 and synergy 3 represented ventral trunk musculature activation with the highest weights representing mid and lower thoracic muscles, synergy 2 represented dorsal trunk musculature activation with the highest weights representing the contralateral upper thoracic longissimus. The synergy scores were compared across coactivation zones to explain the role of the different muscle groups. For example, synergy 1 and synergy 2 explain the difference between FLT and HLT coactivation zones. Specifically, synergy 1 score of FLT was different from that of HLT by almost exclusive contribution of mid and lower thoracic ventral trunk musculature. Alternatively, the scores for synergy 2 were different between all coactivation zones, primarily through contribution of upper thoracic dorsal trunk musculature. Synergy 3 scores, whose predominate contribution was also from mid and lower thoracic ventral trunk, were not different between coactivation zones suggesting it might not be possible to explain differences between muscle contribution to exclusively trunk (ET) and contribution to coactivation zones.



Supplemental Figure 2. Exemplar SEPs confirm stronger sensory integration between trunk and hindlimb vs. forelimb. A) Photograph of an animal with the body grid, indicating the electrical stimulation locations (forelimb [FL], mid trunk [MT], hindlimb [HL]). The line running from the ear to tail next to the numbers 1-16 is along the midline of the dorsal trunk and the animal is lying partly on its side. B). Exemplar SEPs recorded in cortical receptive field centers from stimulation to the corresponding body location at 0.5 mA. Supporting results in Fig. 3A, these SEPs show that the electrical stimulation to FL, MT, and HL produce similar responses in each of these body locations' cortical receptive field centers, affirming that electrical stimulation can be used to compare SEPs between different cortical regions. C & D) Exemplar SEPs from HLS1 and FLS1 from stimulation to MT at 0.5 mA (C) and 5.0 mA (D), supporting results from Fig. 3B showing a larger overlap of trunk information in HLS1 compared to FLS1. E) Average SEP amplitudes recorded from upper TrS1 during 5.0 mA stimulation to FL (N = 3) and HL (N = 3). Example SEPs are shown on the right. No differences in average SEP amplitudes or proportion of responsive cells were found, suggesting that the proximity of body regions likely does not contribute to the increased responsiveness seen in TrS1 during hindlimb stimulation.



Supplemental Figure 3. Current source density analysis supports TrM1 receiving hindlimb proprioceptive information from the thalamus. A 16-channel laminar microelectrode array (A2X16, Neuronexus probe 100  $\mu$ m interelectrode distance) was inserted perpendicularly to a depth of 1.60 mm and LFPs were recorded across the depth of the cortex. Current source density (CSD) provides spatiotemporal information (location, latency) of current sinks (yellow) and sources (blue) to confirm the position of the electrode. CSD was quantified as the second spatial derivative of SEP response, computed using the standard CSD method (Nicholson and Freeman 1975). Contour plots were generated with CSD toolbox (Pettersen et al. 2006). CSD profile was spatially filtered with a gaussian filter (SD = 0.1 mm). All CSD (measured in  $\mu$ A/mm3) were normalized to the absolute maximum value of the CSD in response window of 100 ms from stimulus onset. Current sinks represent net inward transmembrane current, while current sources represent outward currents. Images were derived from laminar cortical LFP recordings in TrS1 (A) and TrM1 (B) during mid trunk stimulation (5.0 mA), as well as HLS1 (C) and TrM1 (D) during hindlimb stimulation (5.0 mA). Therefore, top panels A and C are the responses in S1 to stimulation of RF center. TrS1 in response to trunk stimulation (A) and HLS1 in response to hindlimb stimulation (C), both receive early current sinks in the granular layers, suggesting fast input directly from the thalamus. During trunk stimulation, TrM1 receives later current sinks in the infragranular layers, suggesting intracortical communication of sensory information from S1 to M1. Alternatively, TrM1 receives an early current sink during HL stimulation, suggesting early proprioceptive information ascending to M1 directly from the VPL of the thalamus.

1103	Acknowledgements
1104	This work was supported by grant R01NS096971 from the National Institutes of Health and
1105	grant 1933751 from the National Science Foundation.

1106	References
1107 1108 1109	Anders C, Wagner H, Puta C, Grassme R, Petrovitch A, Scholle HC. 2007. Trunk muscle activation patterns during walking at different speeds. J Electromyogr Kinesiol. 17:245–252.
1110 1111	Asanuma H, Stoney Jr. SD, Abzug C. 1968. Relationship between afferent input and motor outflow in cat motorsensory cortex. J Neurophys. 31:670–681.
1112 1113 1114 1115	Asboth L, Friedli L, Beauparlant J, Martinez-Gonzalez C, Anil S, Rey E, Baud L, Pidpruzhnykova G, Anderson MA, Shkorbatova P, Batti L, Pagès S, Kreider J, Schneider BL, Barraud Q, Courtine G. 2018. Cortico–reticulo–spinal circuit reorganization enables functional recovery after severe spinal cord contusion. Nat Neurosci. 21:576–588.
1116 1117 1118	Baldwin MKL, Cooke DF, Goldring AB, Krubitzer L. 2018. Representations of fine digit movements in posterior and anterior parietal cortex revealed using long-train intracortical microstimulation in macaque monkeys. Cereb Cortex. 28:4244–4263.
1119 1120 1121	Baldwin MKL, Cooke DF, Krubitzer L. 2017. Intracortical microstimulation maps of motor, somatosensory, and posterior parietal cortex in tree shrews (tupaia belangeri) reveal complex movement representations. Cereb Cortex. 27:1439–1456.
1122 1123 1124	Beaumont E, Guevara E, Dubeau S, Lesage F, Nagai M, Popovic M. 2014. Functional electrical stimulation post-spinal cord injury improves locomotion and increases afferent input into the central nervous system in rats. J Spinal Cord Med. 37:93–100.
1125 1126 1127	Beloozerova IN, Sirota MG, Swadlow HA, Orlovsky GN, Popova LB, Deliagina TG. 2003. Activity of different classes of neurons of the motor cortex during postural corrections. J Neurosci. 23:7844–7853.
1128 1129 1130	Blumenthal GH, Nandakumar B, Schnider AK, Detloff MR, Ricard J, Bethea JR, Moxon KA. 2021. Modelling at-level allodynia after mid-thoracic contusion in the rat. Eur J Pain. 25:801–816.
1131 1132	Boyeson MG, Feeney DM, Dail WG. 1991. Cortical microstimulation thresholds adjacent to sensorimotor cortex injury. J Neurotrauma. 8:205–217.
1133 1134 1135	Bridges NR, Meyers M, Garcia J, Shewokis PA, Moxon KA. 2018. A rodent brain-machine interface paradigm to study the impact of paraplegia on BMI performance. J Neurosci Methods. 306:103–114.
1136 1137	Brink EE, Pfaff DW. 1980. Vertebral muscles of the back and tail of the albino rat (Rattus norvegicus albinus). Brain Behav Evol. 17:1–47.
1138 1139	Brown AR, Teskey GC. 2014. Motor cortex is functionally organized as a set of spatially distinct representations for complex movements. J Neurosci. 34:13574–13585.
1140	Canedo A. 1997. Primary motor cortex influences on the descending and ascending systems.

- 1142 Capogrosso M, Milekovic T, Borton D, Wagner F, Moraud EM, Mignardot JB, Buse N, Gandar
- J, Barraud Q, Xing D, Rey E, Duis S, Jianzhong Y, Ko WK, Li Q, Detemple P, Denison T,
- Micera S, Bezard E, Bloch J, Courtine G. 2016. A brain-spine interface alleviating gait
- deficits after spinal cord injury in primates. Nature. 539:284–288.
- 1146 Chakrabarti S, Zhang M, Alloway KD. 2008. MI neuronal responses to peripheral whisker
- stimulation: Relationship to neuronal activity in SI barrels and septa. J Neurophysiol.
- 1148 100:50–63.
- 1149 Chapin JK. 1986. Laminar differences in sizes, shapes, and response profiles of cutaneous
- receptive fields in the rat SI cortex. Exp Brain Res. 62:549–559.
- 1151 Chapin JK, Lin CS. 1984. Mapping the body representation in the SI cortex of anesthetized and
- awake rats. J Comp Neurol. 229:199–213.
- 1153 Clement EA, Richard A, Thwaites M, Ailon J, Peters S, Dickson CT. 2008. Cyclic and sleep-like
- spontaneous alternations of brain state under urethane anaesthesia. PLoS One. 3:e2004.
- 1155 Cooke DF, Padberg J, Zahner T, Krubitzer L. 2012. The functional organization and cortical
- connections of motor cortex in squirrels. Cereb Cortex. 22:1959–1978.
- Deliagina TG, Beloozerova IN. 2000. Role of different sensory inputs for maintenance of body
- posture in sitting rat and rabbit. Motor Control. 4:439–452.
- Deliagina TG, Zelenin P V., Beloozerova IN, Orlovsky GN. 2007. Nervous mechanisms
- 1160 controlling body posture. Physiol Behav. 92:148–154.
- Donoghue JP, Kerman KL, Ebner FF. 1979. Evidence for two organizational plans within the
- somatic sensory-motor cortex of the rat. J Comp Neurol. 183:647–663.
- Donoghue JP, Wise SP. 1982. The motor cortex of the rat: Cytoarchitecture and
- microstimulation mapping. J Comp Neurol. 212:76–88.
- Edgerton VR, Courtine G, Gerasimenko Y, Lavrov I, Ichiyama R, Fong AJ, Cai LL, Otoshi CK,
- Tillakaratne NJK, Burdick JW, Roy RR. 2008. Training locomotor networks. Brain Res
- 1167 Rev. 57:241–254.
- Farkas T, Kis Z, Toldi J, Wolff JR. 1999. Activation of the primary motor cortex by
- somatosensory stimulation in adult rats is mediated mainly by associational connections
- from the somatosensory cortex. Neuroscience. 90:353–361.
- 1171 Ferezou I, Haiss F, Gentet LJ, Aronoff R, Weber B, Petersen CCH. 2007. Spatiotemporal
- dynamics of cortical sensorimotor integration in behaving mice. Neuron. 56:907–923.
- Foffani G, Chapin JK, Moxon KA. 2008. Computational role of large receptive fields in the
- primary somatosensory cortex. J Neurophysiol. 100:268–280.
- 1175 Foffani G, Moxon KA. 2004. PSTH-based classification of sensory stimuli using ensembles of
- single neurons. J Neurosci Methods. 135:107–120.
- Formento E, Minassian K, Wagner F, Mignardot JB, Le Goff-Mignardot CG, Rowald A, Bloch

- J, Micera S, Capogrosso M, Courtine G. 2018. Electrical spinal cord stimulation must 1178 1179 preserve proprioception to enable locomotion in humans with spinal cord injury. Nat Neurosci. 21:1728-1741. 1180 Francis JT, Xu S, Chapin JK. 2008. Proprioceptive and cutaneous representations in the rat 1181 ventral posterolateral thalamus. J Neurophysiol. 99:2291–2304. 1182 Friedberg MH, Lee SM, Ebner FF. 1999. Modulation of receptive field properties of thalamic 1183 somatosensory neurons by the depth of anesthesia. J Neurophysiol. 81:2243–2252. 1184 Frost SB, Dunham CL, Barbay S, Krizsan-Agbas D, Winter MK, Guggenmos DJ, Nudo RJ. 1185 2015. Output properties of the cortical hindlimb motor area in spinal cord-injured rats. J 1186 Neurotrauma. 32:1666-1673. 1187 Ganzer PD, Manohar A, Shumsky JS, Moxon KA. 2016. Therapy induces widespread 1188 reorganization of motor cortex after complete spinal transection that supports motor 1189 recovery. Exp Neurol. 279:1–12. 1190 Ghosh A, Sydekum E, Haiss F, Peduzzi S, Zörner B, Schneider R, Baltes C, Rudin M, Weber B, 1191 1192 Schwab ME. 2009. Functional and anatomical reorganization of the sensory-motor cortex 1193 after incomplete spinal cord injury in adult rats. J Neurosci. 29:12210–12219. 1194 Gioanni Y, Lamarche M. 1985. A reappraisal of rat motor cortex organization by intracortical microstimulation. Brain Res. 344:49-61. 1195 1196 Girgis J, Merrett D, Kirkland S, Metz GAS, Verge V, Fouad K. 2007. Reaching training in rats with spinal cord injury promotes plasticity and task specific recovery. Brain. 130:2993– 1197 3003. 1198 Giszter S, Davies MR, Ramakrishnan A, Udoekwere UI, Kargo WJ. 2008. Trunk sensorimotor 1199 1200 cortex is essential for autonomous weight-supported locomotion in adult rats spinalized as 1201 P1/P2 neonates. J Neurophysiol. 100:839–851. Giszter SF, Hockensmith G, Ramakrishnan A, Udoekwere UI. 2010. How spinalized rats can 1202 walk: Biomechanics, cortex, and hindlimb muscle scaling--implications for rehabilitation. 1203 Ann N Y Acad Sci. 1198:279-293. 1204 Giszter SF, Kargo WJ, Davies M, Shibayama M. 1998. Fetal transplants rescue axial muscle 1205 representations in M1 cortex of neonatally transected rats that develop weight support. J 1206 Neurophysiol. 80:3021-3030. 1207 Graziano MSA, Taylor CSR, Moore T. 2002. Complex movements evoked by microstimulation 1208 of precentral cortex. Neuron. 34:841–851. 1209 1210 Griffin DM, Hudson HM, Belhaj-Saif A, Cheney PD. 2014. EMG activation patterns associated
- Hall RD, Lindholm EP. 1974. Organization of motor and somatosensory neocortex in the albino rat. Brain Res. 66:23–38.

1212

Neurosci. 34:1647-1656.

with high frequency, long-duration intracortical microstimulation of primary motor cortex. J

- Halley AC, Baldwin MKL, Cooke DF, Englund M, Krubitzer L. 2020. Distributed motor control
- of limb movements in rat motor and somatosensory cortex: The sensorimotor amalgam
- revisited. Cereb Cortex. 30:6296–6312.
- Harkema S, Gerasimenko Y, Hodes J, Burdick J, Angeli C, Chen Y, Ferreira C, Willhite A, Rejc
- E, Grossman RG, Reggie Edgerton V. 2011. Effect of epidural stimulation of the
- lumbosacral spinal cord on voluntary movement, standing, and assisted stepping after motor
- complete paraplegia: A case study. Lancet. 377:1938–1947.
- Hekmatpanah J. 1961. Organization of tactile dermatomes, C1 through L4, in cat. J
- 1223 Neurophysiol. 24:129–140.
- Hicks SP, D'Amato CJ. 1975. Motor-sensory cortex-corticospinal system and developing
- locomotion and placing in rats. Am J Anat. 143:1–42.
- Hodges PW. 2001. Changes in motor planning of feedforward postural responses of the trunk
- muscles in low back pain. Exp Brain Res. 141:261–266.
- Hooks BM. 2016. Sensorimotor convergence in circuitry of the motor cortex. Neuroscientist.
- 1229 23:251–263.
- Hooks BM, Mao T, Gutnisky DA, Yamawaki N, Svoboda K, Shepherd GMG. 2013.
- Organization of cortical and thalamic input to pyramidal neurons in mouse motor cortex. J
- 1232 Neurosci. 33:748–760.
- Horak FB, Jacobs J V. 2007. Cortical control of postural responses. J Neural Transm. 114:1339–
- 1234 1348.
- Humanes-Valera D, Aguilar J, Foffani G. 2013. Reorganization of the intact somatosensory
- cortex immediately after spinal cord injury. PLoS One. 8:e69655.
- Hummelsheim H, Wiesendanger M. 1985. Is the hindlimb representation of the rat's cortex a
- "sensorimotor amalgam"? Brain Res. 346:75–81.
- 1239 Ingemanson ML, Rowe JR, Chan V, Wolbrecht ET, Reinkensmeyer DJ, Cramer SC. 2019.
- Somatosensory system integrity explains differences in treatment response after stroke.
- 1241 Neurology. 92:e1098–e1108.
- 1242 Itomi K, Kakigi R, Maeda K, Hoshiyama M. 2000. Dermatome versus homunculus; detailed
- topography of the primary somatosensory cortex following trunk stimulation. Clin
- 1244 Neurophysiol. 111:405–412.
- Kao T, Shumsky JS, Murray M, Moxon KA. 2009. Exercise induces cortical plasticity after
- neonatal spinal cord injury in the rat. J Neurosci. 29:7549–7557.
- Karayannidou A, Zelenin P V., Orlovsky GN, Sirota MG, Beloozerova IN, Deliagina TG. 2009.
- Maintenance of lateral stability during standing and walking in the cat. J Neurophysiol.
- 1249 101:8–19.
- 1250 Kargo WJ, Nitz DA. 2003. Early skill learning is expressed through selection and tuning of

- 1251 cortically represented muscle synergies. J Neurosci. 23:11255–11269.
- 1252 Kirk EJ. 1968. The dermatomes of the sheep. J Comp Neurol. 134:353–369.
- 1253 Kirk EJ, Denny-Brown D. 1970. Functional variation in dermatomes in the macaque monkey 1254 following dorsal root lesions. J Comp Neurol. 139:307–320.
- Knudsen EB, Moxon KA. 2017. Restoration of hindlimb movements after complete spinal cord injury using brain-controlled functional electrical stimulation. Front Neurosci. 11:715.
- Kuhn RA. 1953. Organization of tactile dermatomes in cat and monkey. J Neurophysiol. 16:169–1258 182.
- Kunori N, Takashima I. 2016. High-order motor cortex in rats receives somatosensory inputs from the primary motor cortex via cortico-cortical pathways. Eur J Neurosci. 44:2925–2934.
- Leergaard TB, Alloway KD, Pham TAT, Bolstad I, Hoffer ZS, Pettersen C, Bjaalie JG. 2004.

  Three-dimensional topography of corticopontine projections from rat sensorimotor cortex:
- 1264 Comparisons with corticostriatal projections reveal diverse integrative organization. J Comp
- 1265 Neurol. 478:306–322.
- Lemieux M, Josset N, Roussel M, Couraud S, Bretzner F. 2016. Speed-dependent modulation of the locomotor behavior in adult mice reveals attractor and transitional gaits. Front Neurosci. 10:42.
- Lenschow C, Brecht M. 2018. Physiological and anatomical outputs of rat genital cortex. Cereb Cortex. 28:1472–1486.
- Li CX, Waters RS. 1991. Organization of the mouse motor cortex studied by retrograde tracing and intracortical microstimulation (ICMS) mapping. Can J Neurol Sci. 18:28–38.
- Lilja J, Endo T, Hofstetter C, Westman E, Young J, Olson L, Spenger C. 2006. Blood
- oxygenation level-dependent visualization of synaptic relay stations of sensory pathways
- along the neuroaxis in response to graded sensory stimulation of a limb. J Neurosci.
- 1276 26:6330<del>-</del>6336.
- Liu C, Foffani G, Scaglione A, Aguilar J, Moxon KA. 2017. Adaptation of thalamic neurons
- provides information about the spatiotemporal context of stimulus history. J Neurosci.
- **37:10012–10021.**
- Lombard MC, Nashold BS, Denise Albe-Fessard, Salman N. 1979. Deafferentation
- hypersensitivity in the rat after dorsal rhizotomy: A possible animal model of chronic pain.
- 1282 Pain. 6:163–174.
- Manohar A, Flint RD, Knudsen E, Moxon KA. 2012. Decoding hindlimb movement for a brain machine interface after a complete spinal transection. PLoS One. 7:e52173.
- Manohar A, Foffani G, Ganzer PD, Bethea JR, Moxon KA. 2017. Cortex-dependent recovery of unassisted hindlimb locomotion after complete spinal cord injury in adult rats. Elife.

- 6:e23532. 1287 Mao T, Kusefoglu D, Hooks BM, Huber D, Petreanu L, Svoboda K. 2011. Long-range neuronal 1288 circuits underlying the interaction between sensory and motor cortex. Neuron. 72:111–123. 1289 Megevand P, Troncoso E, Quairiaux C, Muller D, Michel CM, Kiss JZ. 2009. Long-term 1290 1291 plasticity in mouse sensorimotor circuits after rhythmic whisker stimulation. J Neurosci. 29:5326-5335. 1292 Morales-Botello ML, Aguilar J, Foffani G. 2012. Imaging the spatio-temporal dynamics of 1293 supragranular activity in the rat somatosensory cortex in response to stimulation of the 1294 paws. PLoS One. 7:e40174. 1295 1296 Moreno-López Y, Olivares-Moreno R, Cordero-Erausquin M, Rojas-Piloni G. 2016. Sensorimotor integration by corticospinal system. Front Neuroanat. 10:24. 1297 Murray AJ, Croce K, Belton T, Akay T, Jessell TM. 2018. Balance control mediated by 1298 1299 vestibular circuits directing limb extension or antagonist muscle co-activation. Cell Rep. 22:1325-1338. 1300 Neafsey EJ, Bold EL, Haas G, Hurley-Gius KM, Quirk G, Sievert CF, Terreberry RR. 1986. The 1301 organization of the rat motor cortex: A microstimulation mapping study. Brain Res Rev. 1302 1303 11:77–96. Nicholson C, Freeman JA. 1975. Theory of current source density analysis and determination of 1304 conductivity tensor for anuran cerebellum. J Neurophysiol. 38:356–368. 1305 Overduin SA, d'Avella A, Carmena JM, Bizzi E. 2014. Muscle synergies evoked by 1306 microstimulation are preferentially encoded during behavior. Front Comput Neurosci. 8:20. 1307 Oza CS, Giszter SF. 2014. Plasticity and alterations of trunk motor cortex following spinal cord 1308 1309 injury and non-stepping robot and treadmill training. Exp Neurol. 256:57-69. Oza CS, Giszter SF. 2015. Trunk robot rehabilitation training with active stepping reorganizes 1310 1311 and enriches trunk motor cortex representations in spinal transected rats. J Neurosci. 35:7174–7189. 1312 Paxinos G, Watson C. 2007. The rat brain in stereotaxic coordinates. 6th ed. San Diego (CA): 1313 Academic Press. 1314 Pettersen KH, Devor A, Ulbert I, Dale AM, Einevoll GT. 2006. Current-source density 1315 estimation based on inversion of electrostatic forward solution: Effects of finite extent of 1316 neuronal activity and conductivity discontinuities. J Neurosci Methods. 154:116–133. 1317 1318 Ramanathan D, Conner JM, Tuszynski MH. 2006. A form of motor cortical plasticity that correlates with recovery of function after brain injury. Proc Natl Acad Sci U S A. 1319 103:11370-11375. 1320
- Rejc E, Angeli CA, Atkinson D, Harkema SJ. 2017. Motor recovery after activity-based training with spinal cord epidural stimulation in a chronic motor complete paraplegic. Sci Rep.

7:13476. 1323 Rosén I, Asanuma H. 1972. Peripheral afferent inputs to the forelimb area of the monkey motor 1324 1325 cortex: Input-output relations. Exp Brain Res. 14:257–273. Rossignol S, Dubuc R, Gossard J-P. 2006. Dynamic sensorimotor interactions in locomotion. 1326 1327 Physiol Rev. 86:89-154. Seelke AMH, Dooley JC, Krubitzer LA. 2012. The emergence of somatotopic maps of the body 1328 1329 in s1 in rats: The correspondence between functional and anatomical organization. PLoS One. 7:e32322. 1330 Sherrington CS. 1892. Experiments in examination of the peripheral distribution of the fibres of 1331 the posterior roots of some spinal nerves. Proc R Soc London. 52:333–337. 1332 Smith CL. 1986. Sensory neurons supplying touch domes near the body midlines project 1333 bilaterally in the thoracic spinal cord of rats. J Comp Neurol. 245:541–552. 1334 Smith JB, Alloway KD. 2013. Rat whisker motor cortex is subdivided into sensory-input and 1335 motor-output areas. Front Neural Circuits. 7:4. 1336 Song W, Cajigas I, Brown EN, Giszter SF. 2015. Adaptation to elastic loads and BMI robot 1337 controls during rat locomotion examined with point-process GLMs. Front Syst Neurosci. 1338 9:62. 1339 Stepniewska I, Fang P-C, Kaas JH. 2005. Microstimulation reveals specialized subregions for 1340 different complex movements in posterior parietal cortex of prosimian galagos. Proc Natl 1341 Acad Sci U S A. 102:4878-4883. 1342 Takahashi Y, Nakajima Y, Sakamoto T. 1994. Dermatome mapping in the rat hindlimb by 1343 electrical stimulation of the spinal nerves. Neurosci Lett. 168:85-88. 1344 Takeoka A, Vollenweider I, Courtine G, Arber S. 2014. Muscle spindle feedback directs 1345 locomotor recovery and circuit reorganization after spinal cord injury. Cell. 159:1626–1639. 1346 Tandon S, Kambi N, Jain N. 2008. Overlapping representations of the neck and whiskers in the 1347 rat motor cortex revealed by mapping at different anaesthetic depths. Eur J Neurosci. 1348 27:228-237. 1349 Tandon S, Kambi N, Mohammed H, Jain N. 2013. Complete reorganization of the motor cortex 1350 of adult rats following long-term spinal cord injuries. Eur J Neurosci. 38:2271–2279. 1351 Tsao H, Galea MP, Hodges PW. 2008. Reorganization of the motor cortex is associated with 1352 postural control deficits in recurrent low back pain. Brain. 131:2161–2171. 1353 Tsao H, Tucker KJ, Hodges PW. 2011. Changes in excitability of corticomotor inputs to the 1354 trunk muscles during experimentally-induced acute low back pain. Neuroscience. 181:127– 1355 1356 133. Tutunculer B, Foffani G, Himes BT, Moxon KA. 2006. Structure of the excitatory receptive 1357

1358

fields of infragranular forelimb neurons in the rat primary somatosensory cortex responding

1359	to touch. Cereb Cortex. 16:791–810.
1360 1361 1362 1363	<ul> <li>Van Den Brand R, Heutschi J, Barraud Q, DiGiovanna J, Bartholdi K, Huerlimann M, Friedli L, Vollenweider I, Moraud EM, Duis S, Dominici N, Micera S, Musienko P, Courtine G. 2012. Restoring voluntary control of locomotion after paralyzing spinal cord injury. Science (80-). 336:1182–1185.</li> </ul>
1364 1365	Welker C. 1971. Microelectrode delineation of fine grain somatotopic organization of SmI cerebral neocortex in albino rat. Brain Res. 26:259–275.
1366 1367	Wessels WJT, Feirabend HKP, Marani E. 1994. The rostrocaudal organization in the dorsal root ganglia of the rat: A consequence of plexus formation? Anat Embryol (Berl). 190:1–11.
1368 1369	Whelan PJ. 2009. The involvement of the motor cortex in postural control: A delicate balancing act. J Physiol. 587:3753.
1370 1371	Xerri C, Stern J, Merzenich M. 1994. Alterations of the cortical representation of the rat ventrum induced by nursing behavior. J Neurosci. 14:1710–1721.
1372 1373 1374	Yagüe JG, Humanes-Valera D, Aguilar J, Foffani G. 2014. Functional reorganization of the forepaw cortical representation immediately after thoracic spinal cord hemisection in rats. Exp Neurol. 257:19–24.
1375 1376 1377	Young NA, Vuong J, Flynn C, Teskey GC. 2011. Optimal parameters for microstimulation derived forelimb movement thresholds and motor maps in rats and mice. J Neurosci Methods. 196:60–69.
1378	